



MONTCLAIR STATE
UNIVERSITY

Montclair State University
**Montclair State University Digital
Commons**

Department of Earth and Environmental Studies Faculty Scholarship and Creative Works Department of Earth and Environmental Studies

2010

Geochemical Investigation of an Offshore Sewage Sludge Deposit, Barcelona, Catalonia, Spain


Michael A. Kruge
Montclair State University, krugem@mail.montclair.edu

Albert Permanyer
University of Barcelona

Jordi Serra
University of Barcelona

Danlin Yu
Montclair State University

Follow this and additional works at: <https://digitalcommons.montclair.edu/earth-environ-studies-facpubs>

 Part of the [Analytical Chemistry Commons](#), [Environmental Chemistry Commons](#), [Environmental Sciences Commons](#), [Geochemistry Commons](#), and the [Geophysics and Seismology Commons](#)

MSU Digital Commons Citation

Kruge, Michael A.; Permanyer, Albert; Serra, Jordi; and Yu, Danlin, "Geochemical Investigation of an Offshore Sewage Sludge Deposit, Barcelona, Catalonia, Spain" (2010). *Department of Earth and Environmental Studies Faculty Scholarship and Creative Works*. 82.
<https://digitalcommons.montclair.edu/earth-environ-studies-facpubs/82>

This Article is brought to you for free and open access by the Department of Earth and Environmental Studies at Montclair State University Digital Commons. It has been accepted for inclusion in Department of Earth and Environmental Studies Faculty Scholarship and Creative Works by an authorized administrator of Montclair State University Digital Commons. For more information, please contact digitalcommons@montclair.edu.

Preprint: Kruge M.A., Permanyer A., Serra J., Yu D. (2010) Geochemical investigation of an offshore sewage sludge deposit, Barcelona, Catalonia, Spain. *Journal of Analytical and Applied Pyrolysis* **89**:204-217. <https://doi.org/10.1016/j.jaap.2010.08.005>

Geochemical Investigation of an Offshore Sewage Sludge Deposit, Barcelona, Catalonia, Spain

M. A. Kruge^{1*}, A. Permanyer², J. Serra² and D. Yu¹

¹Department of Earth and Environmental Studies, Montclair State University, Montclair, NJ, 07043 USA

²Facultat de Geologia, Universitat de Barcelona, 08028 Barcelona, Catalonia, Spain

* Corresponding author. Tel.: +1-973-655-7902, e-mail: krugem@mail.montclair.edu

Abstract

For 20 years ending in the 1990's the city of Barcelona discharged the products from a large primary sewage treatment plant directly into the Mediterranean Sea via underwater conduits. About ca. 3 million m³ of relict sewage sludge, rich in organic matter and heavy metals, has spread over an elongated area offshore, due to successive ruptures of the conduits. The use of the discharge pipes ceased, but the sludge deposit remains in place for the time being.

To understand the history and present state of the sludge deposit in advance of future remediation, a program of geophysical mapping, sampling, and analytical work was undertaken. Rock Eval pyrolysis, although created for use in petroleum prospecting, can also be applied to environmental contamination studies. It offers a simple means to effectively delineate the sludge deposit, with the S₂ parameter and the hydrogen and oxygen indices particularly useful. On the molecular level, the sludge flash pyrolysis products notably include relatively abundant C₂₇ and C₂₉ sterenes and steranes, likely produced from the pyrolysis of fecal and other steroids, including coprostanol, in the sewage sludge. Linear alkylbenzenes and trialkylamines, derived from surfactant residues in the sludge, are also detected. The indoles detected are likely the pyrolysis products of proteins, while the alkylnitriles and alkylamides in the pyrolyzate likely derive from bacterial biomass. Principal components analysis aided the interpretation of the large geochemical dataset and a geographic information system enabled the three-dimensional visualization of the results in their geospatial context. The distinctive pyrolysis products and the trace elements would be geochemical markers useful in planning and assessing a future remediation program. The recognition of a distinctive sewage pyrolysis-GC/MS signature in this deposit would facilitate the use of this method in the detection of sewage-contaminated sediments in urban waterways worldwide.

Key words: organic pollution; urban waterways; pyrolysis-GC/MS; geographic information system; steroids; Rock Eval pyrolysis

1. Introduction

For over 25 years, the main sewage treatment plant serving Barcelona and a portion of its metropolitan area discharged its sludge seawards, after only primary treatment. The plant was situated near the southern bank at the mouth of the Besòs River (Fig.1) and operated from the 1970's through the late 1990's. Throughout its period of operation, the plant operators modified the treatment methods as stipulated by legislation, finally ceasing marine discharge, in accordance with European environmental regulations.

[Figure 1]

Figure 1. Location map showing the extent of the offshore sewage sludge ("mud") plume relative to the outfall conduits and the locations of the cores. Water depth, dominant marine current direction and calcium ion concentrations in surface sediment are given (based on 30 surface sediment grab samples).

The plant discharged its sludge, rich in organic matter and metals, 3 km offshore via an underwater pipe, at a water depth of 55 m. Treated water was discharged via a parallel pipe (Fig. 1). Fishing trawlers ruptured the sludge pipe on several occasions during its period of operation. These accidents triggered sludge discharges in shallower water closer to shore, at depths less than 40 m as near as 1.5 km from the coast. The present shape of the sludge deposit is a function of the location of the rupture points along the pipe, with a lobate southwestern edge due to the prevailing southwesterly marine current (Fig. 1). The sludge deposit remains in place for the time being because the flocculation treatment it received gave it a sticky "chocolate mousse" texture, imparting resistance to resuspension on the seabed. This is evidenced by its tendency to preserve the surface markings left by marine organisms and trawling.

Environmentally, the concern is that the sludge could be a source of pollution to the nearshore waters and habitats. Thus, the objective of this research is to determine the present state of the deposit and its possible future evolution, in terms of, for example, contaminant type and concentrations, ion exchange, migration, and mineralization.

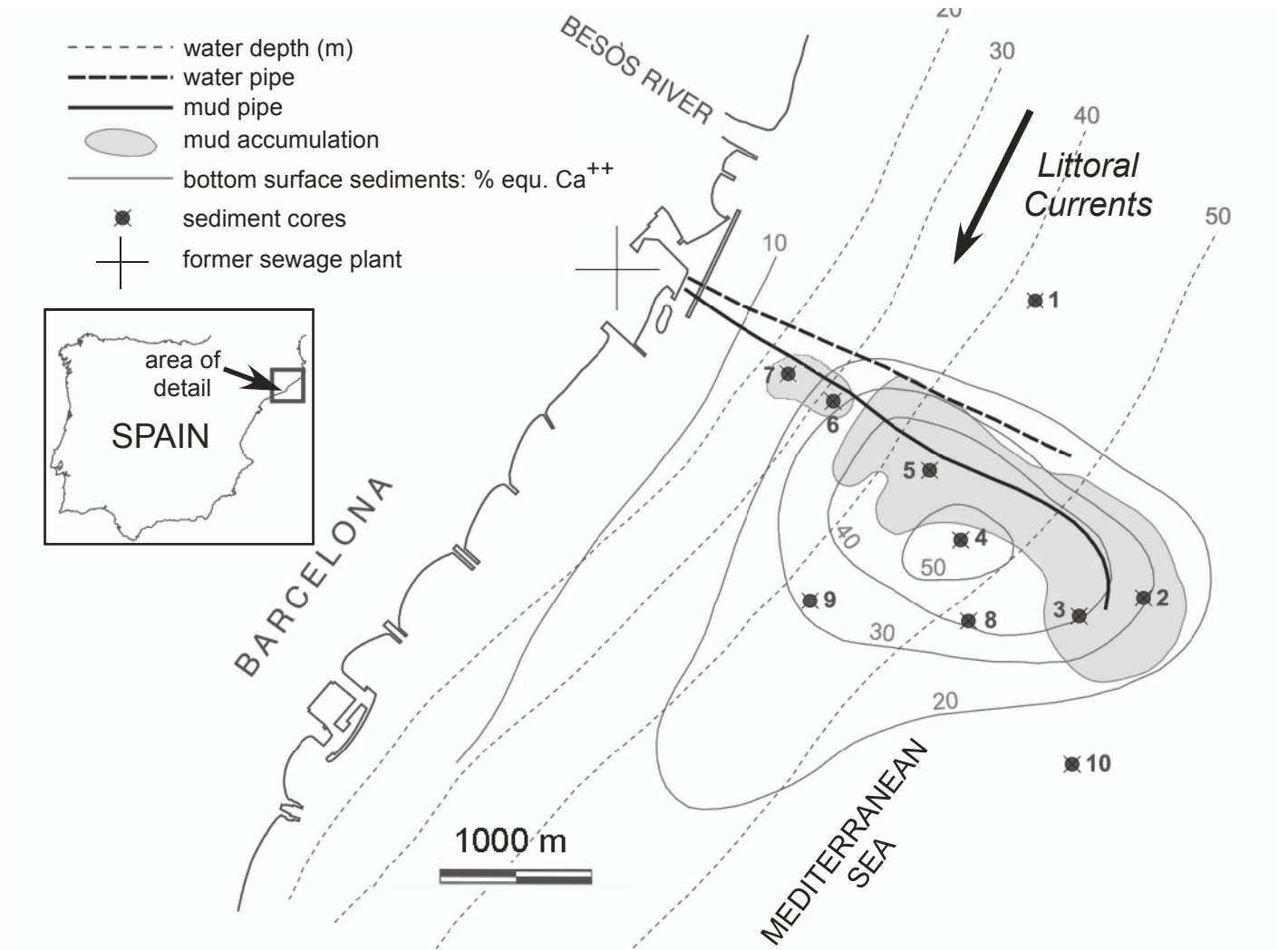
Most previous sewage sludge pyrolysis studies have been concerned with lower molecular weight compounds, production of gaseous and liquid fuels by large-scale pyrolysis, and waste reduction to reduce disposal costs [1-4]. In the present study, bulk pyrolysis with flame ionization and thermal conductivity detectors (Rock Eval) and analytical pyrolysis-GC/MS were used to delineate a submarine sewage sludge deposit, as well as to ascertain chemical signatures that would be useful in the detection of sewage contamination in other urban waterways.

2. Methods

2.1. Field work and sampling

The first step in characterizing this deposit was to determine its spatial distribution (boundaries, area, and volume). Towards this end, geophysical and sedimentological work

Fig. 1



was undertaken using seismic and side scan sonar (Hydroscan Klein 595), covering a 30 km² area. A vibrocorer (Rossfelder Corp.) and Van Veen dredge were used as sampling devices.

A series of 10 sediment cores over 2 m in length were collected by vibrocorer from the Mediterranean seabed near Barcelona (Fig. 1). The vibrocoreing induced mechanical compaction of the sludge by a factor of about 2.5, as determined by correlation with the geophysical data. A total of 44 samples were taken from the 10 cores, sampling the upper, organic-rich layer of sewage sludge, as well as the underlying sediment (Table 1). Samples were dried at ambient temperature and manually homogenized. An additional 30 surface sediment dredge samples were collected to determine the extent of sludge transport by the prevailing longshore current.

[Table 1]

Table 1. Sample identification, major and trace element concentrations, and Rock Eval pyrolysis results.

2.2. Elemental analysis

The raw, disaggregated, dry core sediment was analyzed for total organic carbon (C_{org}) content using a Leco instrument. Elemental analyses were performed by Activation Laboratories, Ltd. of Ancaster (ON) Canada. Sulfur and phosphorus were determined by inductively coupled plasma optical emission spectroscopy (ICP-OES) and metals by inductively coupled plasma mass spectrometry (ICP-MS) following aqua regia extraction (Table 1). U.S.G.S. analytical standards GXR-1, 2, 4 and 6 were employed. Sediment samples were analyzed by a Rock Eval II instrument, following standard petroleum source rock procedures (initial temperature 300 °C, isothermal for 3 min., temperature gradient 25 °C/min., S_3 analysis selected, trap stop 390 °C, oxidation time 7 min.). The 30 surface dredge samples were only analyzed for texture, calcium content (using a Bernard calcimeter), and total organic matter.

2.3. Pyrolysis-Gas Chromatography/Mass Spectrometry

Pyrolysis-gas chromatography/mass spectrometry (Py-GC/MS) was performed using a CDS 120 pyroprobe, coupled to a HP 5890 gas chromatograph with a HP 5970 mass selective detector and a 50 m J&W Scientific DB-5MS column (0.2mm i.d., film thickness 0.33 μ m). A measured amount (a few mg) of dry, powdered sample was pyrolyzed in a flow of helium for 20 sec. in a platinum coil at 600 °C, as measured by a thermocouple in the sample holder. The GC oven was operated under the following program: isothermal for 5 min at 40 °C; temperature programmed at 5 °C/min. to 300 °C and then isothermal for 30 min. The MS was operated in either full scan (50-450 Da, 1.21 scans/sec.) or selected ion monitoring (SIM) mode, 70eV ionization voltage. After performing full-scan Py-GC/MS on samples 202, 405, 503, 508, and 701, the full suite of samples was analyzed with the mass spectrometer in selected ion monitoring (SIM) mode. The ions for the SIM mode (Table 2) were chosen based on study of the full scan results, to be sure that all major compounds are represented, as

well as trace components such as PAHs and hopanes. The SIM approach improved sensitivity in detection of these target trace analytes, particularly in samples poor in organic matter.

Sample 503 was reanalyzed using a CDS 2000 pyroprobe, coupled to a Thermo Finnigan Focus DSQ GC/MS and a 60 m J&W Scientific DB-1MS column (0.25 mm i.d., film thickness 0.25 μm). The GC oven was operated under the following program: isothermal for 5 min at 50 $^{\circ}\text{C}$; temperature programmed at 5 $^{\circ}\text{C}/\text{min}$. to 300 $^{\circ}\text{C}$ and then isothermal for 25 min. The MS was operated in full scan mode (50-500 Da, 1.08 scans/sec.) The sample was heated in the pyroprobe at 300 $^{\circ}\text{C}$ for 20 sec (essentially, thermodesorption of semi-volatile compounds), followed by a full GC run. Without removing the pyroprobe from the interface, a second GC run commenced, this time with the sample heated at 610 $^{\circ}\text{C}$ for 20 sec (“sequential pyrolysis”). Sample 503 was also reanalyzed with this Py-GC/MS system in full scan mode using a shorter column (30 m J&W Scientific DB-1MS column, 0.25 mm i.d., film thickness 0.25 μm) under the following conditions: isothermal for 5 min at 50 $^{\circ}\text{C}$; temperature programmed at 5 $^{\circ}\text{C}/\text{min}$. to 300 $^{\circ}\text{C}$ and then isothermal for 5 min. Pyrolysis was at 610 $^{\circ}\text{C}$ for 20 sec. Freeze-dried cultured *Escherichia coli* was analyzed under these conditions for reference purposes, as an example of a fecal bacterium.

2.4. Data processing

Quantification of Py-GC/MS data was accomplished using Hewlett Packard GC/MS software G1701AA (version A.03.00). Only selected ion monitoring (SIM) data were quantitated. All data were adjusted by response factors previously determined for each compound using this GC/MS instrument and normalized to the values for toluene in each sample. Toluene is a major pyrolysis product of many types of organic matter and is the most abundant compound in the pyrolyzate of every sediment sample in this study. The raw spectrometer counts for toluene (m/z 91), normalized to the weight of sediment pyrolyzed, were found to be proportional to the organic carbon concentrations in these samples ($r^2 = 0.82$ excluding one outlier), as previously noted in a study of Barcelona harbor sediments [5]. The semiquantitative results for individual compounds presented herein may thus be considered to represent geochemically anomalous or “excess” quantities.

Principal components analysis using Rock Eval, major and trace element, and Py-GC/MS data was performed using JMP version 5.1 software (SAS Institute Inc, 2004). The data set was scaled by taking the square root of all values prior to the multivariate analysis.

2.5. Geographic information system

To visually represent the pollutant distribution of the ten sediment cores, the data for 10 key parameters (based on the results of the multivariate analysis) were digitized using ArcGIS® software, and assembled into a geographic database for mapping purposes. First, the data were re-grouped according to each sediment core’s geographic coordinates. For the vertical dimension, twelve 20 cm thick layers were visualized, since the cores were approximately 220 cm long and they were subsampled at 20 cm intervals for the most part.

Then the values of the various parameters at different depths were assigned as attribute values to the appropriate core and layer, filling the three dimensional framework.

The background coastline, water pipes, and bathymetric contours were digitized from an overlaid thematic map that was geo-referenced to align with the sediment cores. To emphasize the visual representation, a vertical bar chart symbolism was chosen in ArcGIS. Null values on these charts indicate absence of data, meaning that no subsamples were taken from those intervals.

3. Results and Discussion

3.1. Geophysical and sedimentological characterization of the sewage sludge deposit

High resolution seismic reflection data (“mud penetrator” mode at 3.5 kHz) showed that the sludge deposit exhibited no internal reflectors, due to the elevated gas content within the sediment leading to absorption of the emitted seismic energy. In contrast, the surrounding natural sediment gave a good seismic response, permitting an accurate determination of the mud deposit area, approximately 3 km². The volume of the deposit was determined to be about 3 X 10⁶ m³, using the seismic profile results and reference base level. The side scan sonar revealed that the sticky “chocolate mousse” texture of the sludge deposit preserves trawling scars, in contrast to the surrounding sediment, upon which trawling marks quickly disappear due to normal sediment transport processes.

The sediments in the cores document the Holocene transgressive sequence, a succession of facies proceeding from basal sands and gravels (age > 8 ka) up to prodeltaic muds (6 ka to present). The recent nearshore sandy facies is present in those cores taken closer to the coast [6]. The organic-rich sewage sludge layer varies in thickness across the deposit, with the maximum (up to 1 m) encountered in cores 2 and 5, corresponding to a real thickness of up to 3 m, accounting for the compaction induced by the coring process. In the other cores the sludge thickness varies with proximity to pipe ruptures and local marine dynamics.

3.2. Geochemical characterization of the sewage sludge deposit

3.2.1. Bulk organic analysis

Based on the results of the geophysical studies, the approximate boundaries of the sewage sludge deposit have been delineated (Fig. 1). This body is long and narrow, following the path of the “mud” outflow pipe from the treatment plant. Had the pipe not ruptured, the sludge accumulation would have only been at the mouth of the pipe, ca. 3 km out to sea. This map also contours the Ca²⁺ concentrations in 30 surface sediment grab samples, the highest values of which coincide with the sludge deposit, but displaced to the southwest, due to transport by the prevailing marine current. Flocculants containing calcium were added during the sewage treatment process and Ca²⁺ serves as a convenient marker for tracing the extent of the deposit. The dark color of the sewage sludge clearly differentiates it from the underlying, light-colored Holocene sediments (Fig. 2), as did the foul odor that emanated during sample

handling. In the cores, the sludge layer varies in thickness from about a decimeter to more than a meter, after compaction due to vibrocoring. In addition to their high sediment Ca^{2+} concentrations ($>10\%$), the core materials from the sludge zone are enriched in organic carbon ($C_{\text{org}} > \approx 2\%$) (Table 1, Fig. 3). The most affected samples are generally those within the top 1 or 2 decimeters of the cores, except for cores 2 and 5, which penetrated thicker zones of the sludge deposit (Figs. 1, 3, Table 1).

[Figure 2]

Figure 2. Photographs of portions of cores 1, 2, 5 and 6, showing the contact of the dark, organic-rich sludge layer with the lighter-colored sediments below. Core 10 encountered a basal pebble layer at a sediment depth of 210 cm, but no sludge. White circles mark the sampling points in these core segments. Core 5 brightness and contrast enhanced due to poor exposure of original photograph.

[Figure 3]

Figure 3. Cross-plot of sediment organic carbon contents and Ca^{2+} ion concentrations in sediment. Sludge deposit samples exhibit elevated values for both parameters. Samples are numbered as in Table 1.

While it is evident that standard bulk parameters such as C_{org} and Ca concentrations work well to roughly delineate the extent of the sludge deposit, it seemed likely that another bulk analytical technique, Rock Eval pyrolysis, would prove suitable for organic matter characterization in this case. Rock Eval is commonly used in petroleum exploration as a quick and inexpensive, but effective, means of source rock characterization [7-11]. The technique has also been successfully applied to the study of Recent sediments [12,13]. It is used in the present study to characterize and delineate organic pollutants in marine sediments.

Values of Rock Eval S_1 , S_2 , and S_3 all correlate well with C_{org} (Table 1). These Rock Eval parameters attain their maximum values (S_1 of 15.5 - 16.3 mg thermally desorbed HC/g sediment, S_2 of 17.1 - 18.3 mg pyrolyzed HC/g sediment, S_3 of 4.7 - 6.3 mg thermally evolved CO_2 /g sediment) in samples 202, 203 and 501, which coincidentally have the highest C_{org} values of the sample set (5.37-5.91%).

A modified Van Krevelen diagram, cross-plotting the Rock Eval oxygen and hydrogen indices, is commonly used in source rock studies [7-11]. Organic matter in recent sediments tends to be enriched in oxygen relative to C_{org} in kerogen, evidenced by higher oxygen index values [12-14]. When the data from the present study are plotted on a modified Van Krevelen diagram, the sludge deposit samples are clearly delineated, having relatively high hydrogen indices and low oxygen indices (Fig. 4a). Basal sediments, underlying the sludge or outside the affected area, are readily distinguished by their low hydrogen indices and high oxygen indices, as would be expected with oxic surface marine sediments. The inset (Fig. 4b) plots the same data in the context of kerogen type as established by Espitalié and others [7-10], showing the relatively high oxygen contents in the organic matter of these samples. Samples from cores 2 and 5, at the thickest portion of the sludge deposit, have the highest hydrogen indices, while those from the tops of cores 3, 4, 6 and 7 have moderately high values (Fig. 4a). Although core 9 was taken outside the mapped sludge deposit (Fig. 1), its uppermost sample

Fig 2

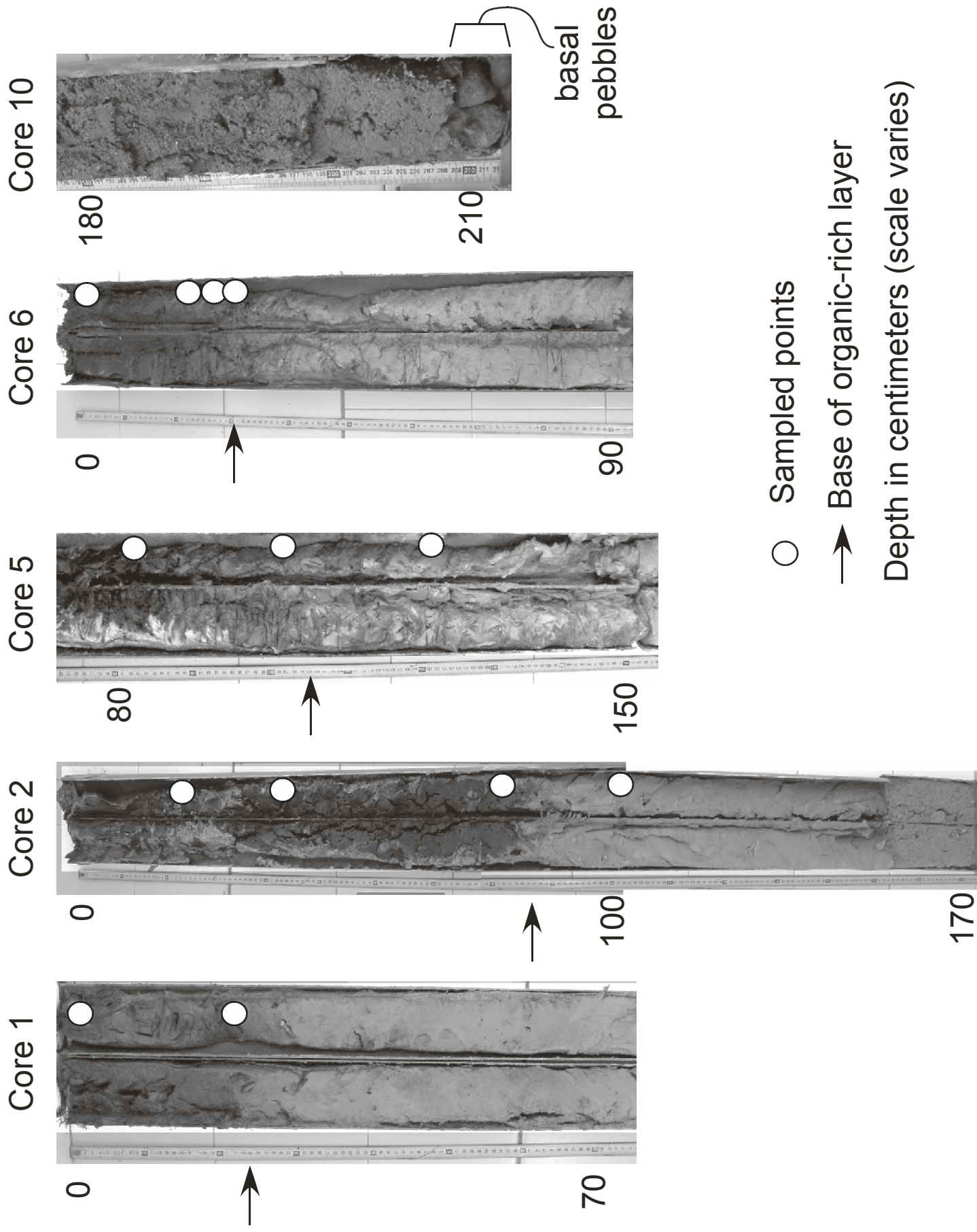
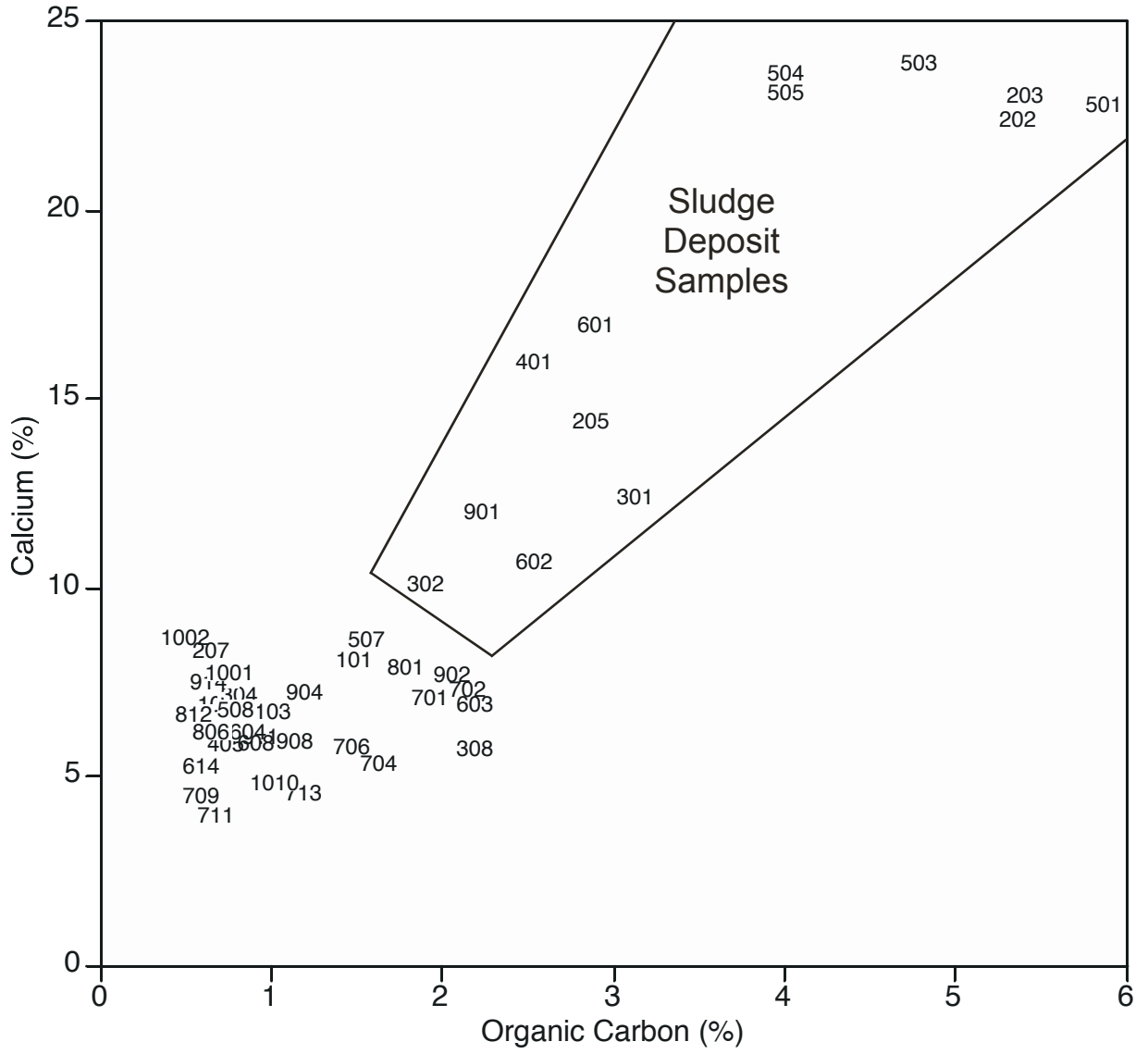


Fig. 3



(901) has a high hydrogen index, offering evidence of downcurrent transport of contaminants. The Rock Eval TOC values of samples 701 and 904 appear too low relative to the standard C_{org} values (Table 1) which are more credible. Since the Rock Eval hydrogen and oxygen values are computed using the Rock Eval TOC in the denominator, the indices derived for these two samples are anomalously high (Table 1) and are not plotted on Figure 4.

[Figure 4]

Figure 4. Modified Van Krevelen diagrams plotting Rock Eval oxygen and hydrogen indices. Samples are numbered as in Table 1. Samples 701 and 904 have anomalously high indices and are not plotted (Table 1; see text). a) Sludge deposits show elevated hydrogen index values, while basal sediments unaffected by the sludge have high oxygen indices. b) The same data as in Fig. 4a, but shown with the kerogen type designations of Espitalié and others [7-10].

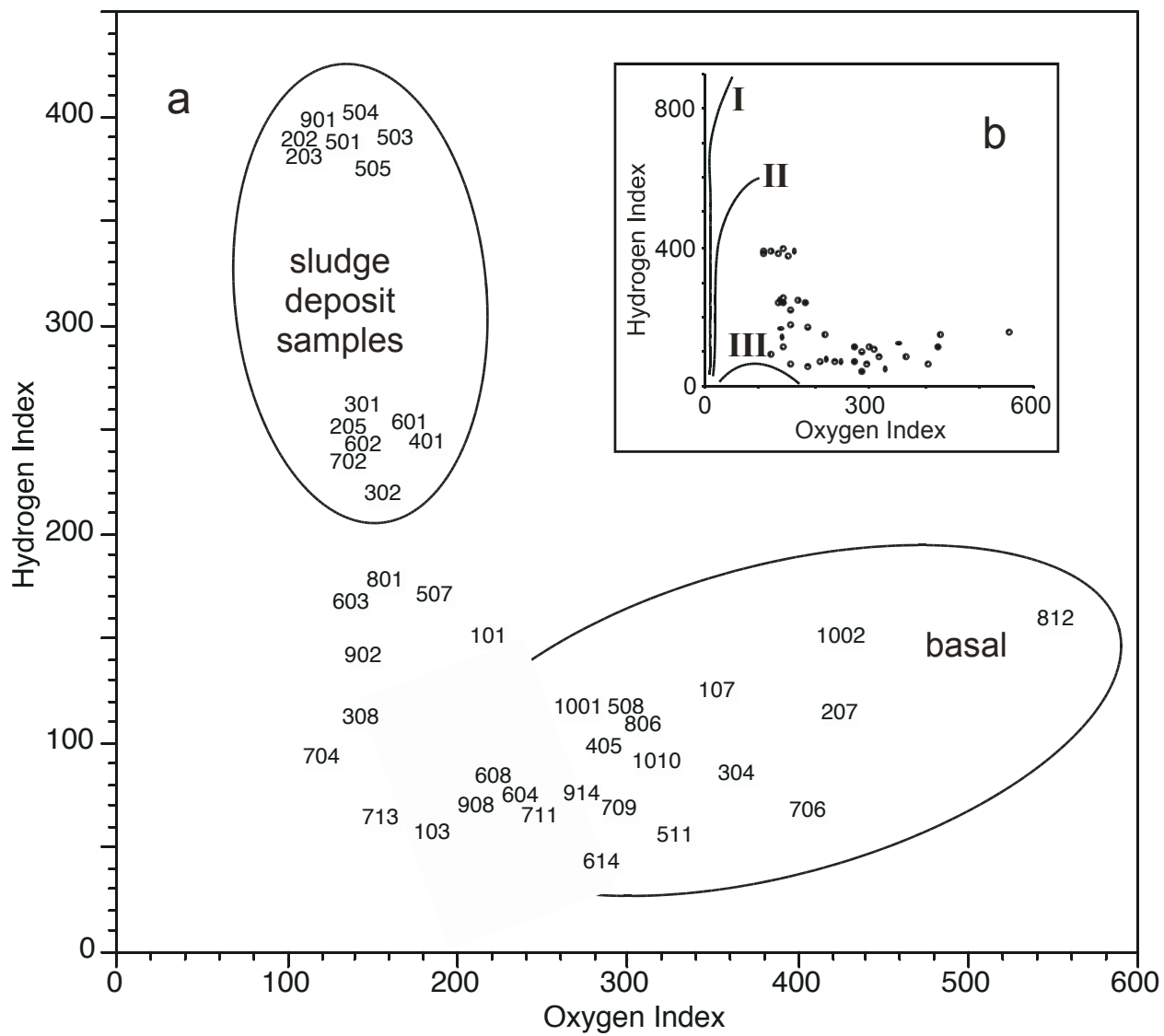
3.2.2. Major and trace elements

As mentioned above, the sludge deposit exhibits elevated C_{org} and Ca concentrations (Fig. 3, Table 1). The sludge deposit is enriched in several other major elements (Na, P and S) but is depleted in Al, Fe, K, Mg and Ti (Table 1), clearly seen in the samples from core 5. Among trace elements, there is enrichment in Ag, Ba, Cd, Cr, Cu, Ni, Pb, Sr and Zn in the sludge but depletion of As, Mn and Zr. B, Be and Co do not exhibit strong trends. The elevated concentrations of the alkaline earth metals may be due to their association with the calcium-based flocculants added during the sewage treatment process. The excess sodium in the sewage sludge may come from household and industrial chemicals, whereas the phosphorus derives from human and food wastes, industrial sources, and detergents. The excess heavy metals in the sludge, often in hundreds of $\mu\text{g g}^{-1}$ and roughly 5 - 20 times greater than background levels in the Holocene sediments at the core bottoms (Table 1), are attributable to industrial input to the waste stream. Although its maximum concentrations are relatively low ($\leq 21 \mu\text{g g}^{-1}$), silver is a particularly useful anthropogenic marker due to its very low background concentrations approaching $0 \mu\text{g g}^{-1}$. It is commonly present in the urban environment due to discharges from photographic and radiographic processes [15]. There is a decrease in concentrations of Cd, Cr and Pb towards the top of several cores (e.g., core 5, Table 1). This is in agreement with the increasingly strict regulation of heavy metal discharges and the gradual elimination of leaded gasoline over the time that the pipe was in operation.

3.2.3. Molecular organic analysis

The suite of core samples was subjected to flash pyrolysis-GC/MS, for a more detailed examination of the nature of the organic matter present. In total, 140 compounds and compound groups were detected in the sediment pyrolyzates (Table 2). Exemplifying the thickest part of the sludge deposit, sample 503 yielded a complex and heterogeneous suite of compounds upon pyrolysis (Fig. 5a). Simple benzenes (peaks **3, 11, 14, 19**), phenols (**18, 22,**

Fig. 4



26) and naphthalenes (**27, 30, 31**) are relatively abundant, but are frequently found in the pyrolyzates of many forms of organic matter and are thus of limited diagnostic value. (Bold-face numbers refer to chromatographic peak numbers in Figures 5-8 and Table 2.) Sample 701 was collected at the nearshore margin of the sludge deposit (Fig. 1) and its pyrolyzate contrasts with that of sample 503. While simple benzenes (**3, 14, 18, 19**) are also important in this pyrolyzate, the sample appears somewhat more aliphatic, with proportionately more *n*-alkanes and *n*-alk-1-enes (Fig. 5b). The humps maximizing at the *n*-C₂₃-C₂₆ retention time range likely indicate the presence of degraded heavy petroleum products in the waste stream (Fig 5a,b), an inference supported by the detection of hopanes in trace quantities.

[Table 2]

Table 2. Compounds detected by Pyrolysis-GC/MS. Peak numbers are those used in the figures. GC retention times from the SIM analysis of representative sample 202 and (where applicable) mass spectral ions used in quantitation are given, as are the compound class groupings used in principal components analysis (PCA). ND: not detected in the SIM analysis of sample 202. NQ: not quantitated.

[Figure 5]

Figure 5. Examples of full scan total ion chromatograms of sediment flash pyrolyzates. See Table 2 for peak number assignments. *n*-Alkane carbon numbers are given in italics below the traces; +: *n*-alkane, ^: *n*-alk-1-ene, X: phthalate contaminants. a) Sample 503 from within the sludge deposit. Note the high relative abundance of the steroids (peaks **98-112**). b) Sample 701 from the shoreward margin of the sludge deposit. Note the prominent peaks corresponding to long-chain organonitrogen compounds (peaks **73, 74, 86, 88**).

3.2.3.1. Organonitrogen compounds

Of greater interest are the organonitrogen compounds, such as pyridine (**1**), pyrrole and methylpyrroles (**2, 9, 10**), and particularly indole and methylindole (**29, 33**), which are relatively very abundant in the sludge deposit pyrolyzate (Fig. 5a). These likely originate from proteinaceous material present in the sludge [16-21], with the indoles particularly diagnostic, as they derive specifically from the pyrolysis of the amino acid tryptophan [22,23]. Indole and methylindole are also major pyrolysis products of cultured *E. coli.*, implying the usefulness of these compounds as markers for the presence of microbial organic matter in sediments. They have previously been detected in the pyrolyzates of sewage sludge studied for biofuel applications [24]. Cyclo-Pro-Pro-diketopiperazine and several other 2,5-diketopiperazines are present in the pyrolyzate of sludge sample 503. These are known pyrolysis products of proteins [25, 26] and are also abundant in the pyrolyzates of freshwater cyanobacteria [27], dairy manure [28], and *E. coli.*

Long-chain alkylnitrogen compounds are also of particular interest in these samples. These comprise three series of compounds, i.e., *n*-alkylnitriles, *n*-alkylamides, and trialkylamines, all with strong even carbon number predominance. Several of these compounds (**74, 86, 88, 90**) are visible on the total ion current trace of the sample 503

Fig. 5a

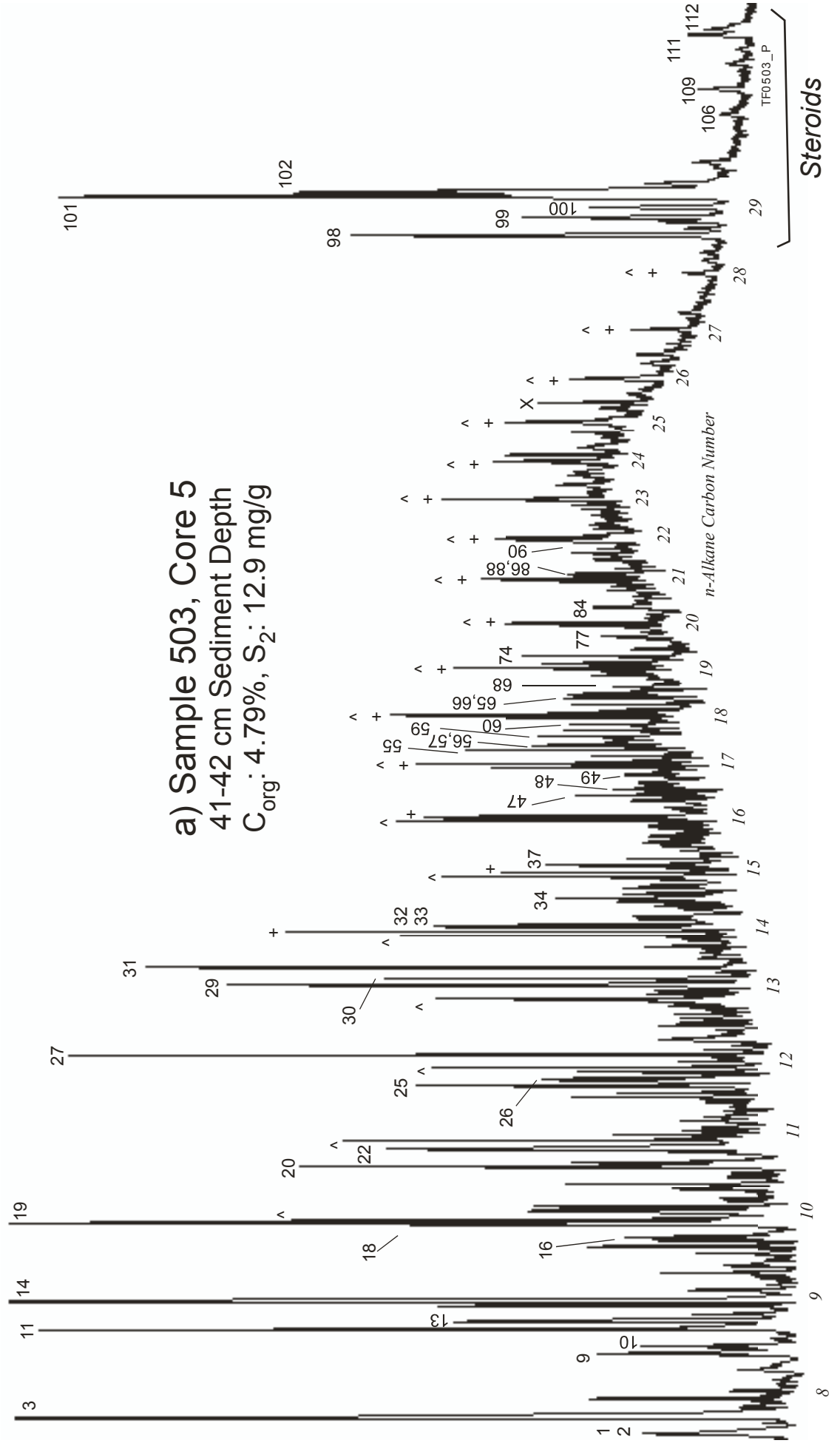


Fig. 5b

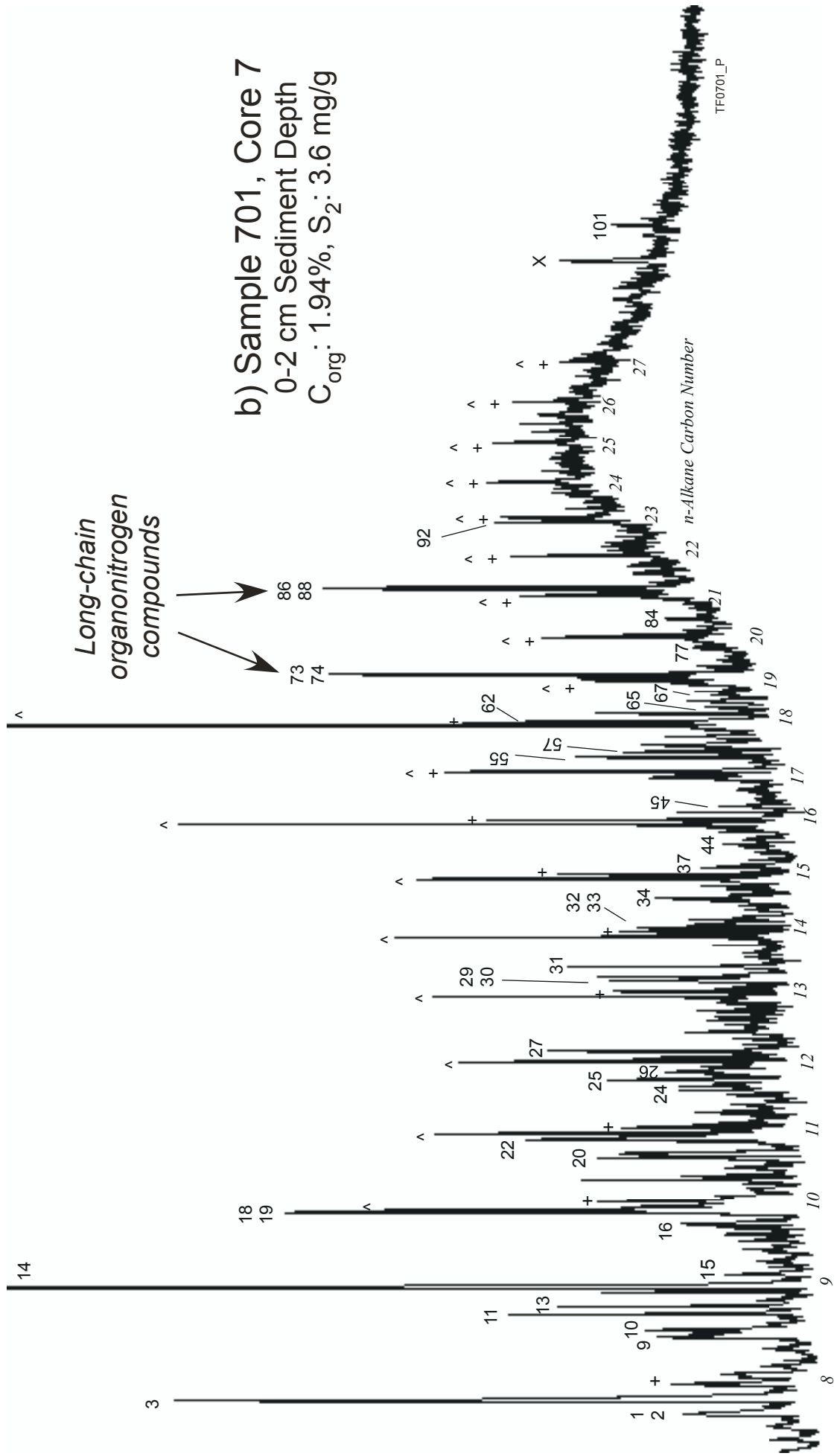


Table 2

Peak	Compound	RT (min)	Quan	PCA	Peak	Compound	RT (min)	Quan	PCA
		TF0202	Ion	Group			TF0202	Ion	Group
1	pyridine	11.71	79	PD	61	1-phenylundecane	45.71	NQ	
2	pyrrole	11.76	67	PL		C18 n-alkane	45.77	71	AL
3	toluene	12.54	91		62	2-hexadecanone	45.97	NQ	
4	2-methylthiophene	12.69	97	T	63	dibenzothiophene	46.14	184	
5	1-methylthiophene	13.05	97	T	64	2-phenyldodecane	46.27	NQ	
	C8 n-alkane	13.82	71	AL	65	6-phenyltridecane	46.53	91	LAB
6	methylpyridine(a)	14.76	93	PD	66	5-phenyltridecane	46.70	91	LAB
7	furancarboxaldehyde	15.44	95	FR	67	phenanthrene	46.80	178	PA
8	cyclopentenone	15.46	82	CP	68	4-phenyltridecane	47.01	91	LAB
9	2-methylpyrrole	15.58	80	PL	69	anthracene	47.07	178	PA
10	3-methylpyrrole	15.91	80	PL	70	3-phenyltridecane	47.62	91	LAB
11	ethylbenzene	16.78	NQ			C19 n-alkane	48.01	71	AL
12	methylpyridine(b)	16.85	93	PD	71	1-phenyldodecane	48.06	NQ	
13	13&14-dimethylbenzenes	17.20	NQ		72	2-heptadecanone	48.16	NQ	
14	styrene	18.08	104		73	n-hexadecanitrile	48.16	69	AN
	C9 n-alkane	18.18	71	AL	74	n-hexadecanamine, N,N-dime	48.17	58	AA
15	3-methylcyclopentenone	18.59	96	CP	75	2-phenyltridecane	48.57	NQ	
16	methylfurancarboxaldehyde	20.95	110	FR	76	3-methylphenanthrene	49.30	192	PA
17	2-methylcyclopentenone	21.13	96	CP	77	2-methylphenanthrene	49.46	192	PA
18	phenol	21.64	94		78	methylanthracene	49.72	192	PA
19	propylene benzene	21.82	NQ		79	n-tetradecamide	49.76	59	AM
	C10 n-alkane	22.22	71	AL	80	9-methylphenanthrene	49.88	192	PA
20	indene	24.46	NQ		81	1-methylphenanthrene	50.03	192	PA
21	2-methylphenol	24.49	107	F		C20 n-alkane	50.13	71	AL
22	4&3-methylphenols	25.24	107	F	82	1-phenyltridecane	50.29	NQ	
23	guaiacol	25.52	124		83	2-octadecanone	50.31	NQ	
	C11 n-alkane	25.93	71	AL	84	phenylnaphthalene	50.91	NQ	
24	2,4-dimethylphenol	27.91	107	F		C21 n-alkane	52.15	71	AL
25	methylindene	28.28	NQ		85	2-nonadecanone	52.31	NQ	
26	4-ethylphenol	28.51	107	F	86	n-octadecanamine, N,N-dimet	52.32	58	AA
	C12 n-alkane	29.35	71	AL	87	dimethylphenanthrenes	52.68	206	PA
27	naphthalene	29.67	128		88	n-octadecanitrile	52.68	69	AN
28	dihydrobenzofuran	30.38	120		89	fluoranthene	53.08	202	PY
	C13 n-alkane	32.54	71	AL	90	n-hexadecamide	53.90	59	AM
29	indole	32.98	117	IL		C22 n-alkane	54.08	71	AL
30	2-methylnaphthalene	33.27	142		91	pyrene	54.31	202	PY
31	1-methylnaphthalene	33.80	142		92	retene	55.72	NQ	
	C14 n-alkane	35.52	71	AL		C23 n-alkane	55.93	71	AL
32	biphenyl	35.76	NQ		93	benzo[a]fluorene	56.01	216	PY
33	methylindole	35.84	130	IL	94	methylpyrenes	57.01	216	PY
34	dimethylnaphthalenes	37.09	156	N		C24 n-alkane	57.70	71	AL
35	2-tridecanone	38.26	NQ		95	n-octadecamide	57.72	59	AM
	C15 n-alkane	38.31	71	AL		C25 n-alkane	59.56	71	AL
36	n-dodecanamine, N,N-dimeth	38.48	58	AA	96	benzo[a]anthracene	60.97	228	CH
37	methylbiphenyl	38.71	NQ		97	chrysene	61.22	228	CH
38	5-phenyldecane	39.40	91	LAB		C26 n-alkane	61.61	71	AL
39	4-phenyldecane	39.66	91	LAB		C27 n-alkane	63.92	71	AL
40	3-phenyldecane	40.25	91	LAB		C28 n-alkane	66.58	71	AL
41	1-phenylnonane	40.71	NQ		98	cholestene1	68.35	215	ST
	C16 n-alkane	40.94	71	AL	99	cholestene2	69.17	NQ	
42	2-tetradecanone	41.15	NQ			C29 n-alkane	69.72	71	AL
43	2-phenyldecane	41.29	NQ		100	cholestene3	70.17	NQ	
44	trimethylnaphthalenes	41.62	170	N	101	cholestene4	70.47	215	ST
45	fluorene	41.69	NQ		102	5- α cholestane (20R)	70.35	217	ST
46	6-phenylundecane	41.84	91	LAB	103	C27 steradiene	ND	NQ	
47	5-phenylundecane	41.94	91	LAB	104	methylcholestene1	71.88	NQ	
48	4-phenylundecane	42.24	91	LAB	105	methylcholestene2	72.88	NQ	
49	3-phenylundecane	42.84	91	LAB	106	methylcholestene3	74.02	NQ	
50	1-phenylundecane	43.22	NQ		107	methylcholestene4	74.44	NQ	
	C17 n-alkane	43.42	71	AL	108	5- α methylcholestane (20R)	74.30	NQ	
51	n-tetradecanitrile	43.45	69	AN	109	ethylcholestene1	75.22	NQ	
52	2-pentadecanone	43.47	NQ		110	ethylcholestene2	76.41	NQ	
53	n-tetradecanamine, N,N-dimet	43.60	58	AA	111	ethylcholestene3	77.77	215	ST
54	2-phenylundecane	43.84	NQ		112	5- α ethylcholestane (20R)	78.03	NQ	
55	prist-1-ene	44.09	69		113	norhopane	79.60	191	HOP
56	6-phenyldodecane	44.25	91	LAB	114	ethylcholestene4	79.18	NQ	
57	5-phenyldodecane	44.37	91	LAB	115	coprostanol	ND	NQ	
58	prist-2-ene	44.41	69		116	C29 steradiene	ND	NQ	
59	4-phenyldodecane	44.71	91	LAB	117	C27 stanone	ND	NQ	
60	3-phenyldodecane	45.29	91	LAB	118	hopane	83.95	191	HOP

pyrolyzate (Fig. 5a) and they produced some of the major peaks (**73, 74, 86, 88**) on the trace from sample 701 (Fig. 5b). Their complete series are more readily seen on individual mass chromatograms, for example, in those from the sample 503 pyrolyzate (Fig. 6). While the summed m/z 69 + 71 trace clearly shows the distribution of *n*-alkanes and *n*-alk-1-enes, along with prist-1-ene, the alkylnitriles (**73, 78**) are also visible (Fig. 6a). These two compounds, which are the C₁₆ and C₁₈ homologues, are distinctive on the m/z 110 trace, along with the C₁₄-alkylnitrile (**51**) (Fig. 6b). The corresponding C₁₄, C₁₆, and C₁₈-alkylamides (**79, 90, 95**) are evident on the m/z 59 trace (Fig. 6c), again demonstrating a marked even carbon number preference. Four trialkylamines with the structure (CH₃)₂NR, for which R is a C₁₂, C₁₄, C₁₆ or C₁₈ alkyl chain (**36, 53, 74, 86**) are prominent on the m/z 58 mass chromatogram (Fig. 6d). The alkan-2-one series from C₁₃ to C₁₉ (**35, 42, 52, 62, 72, 83, 85**) is also evident on this trace, exhibiting a pronounced odd carbon number predominance.

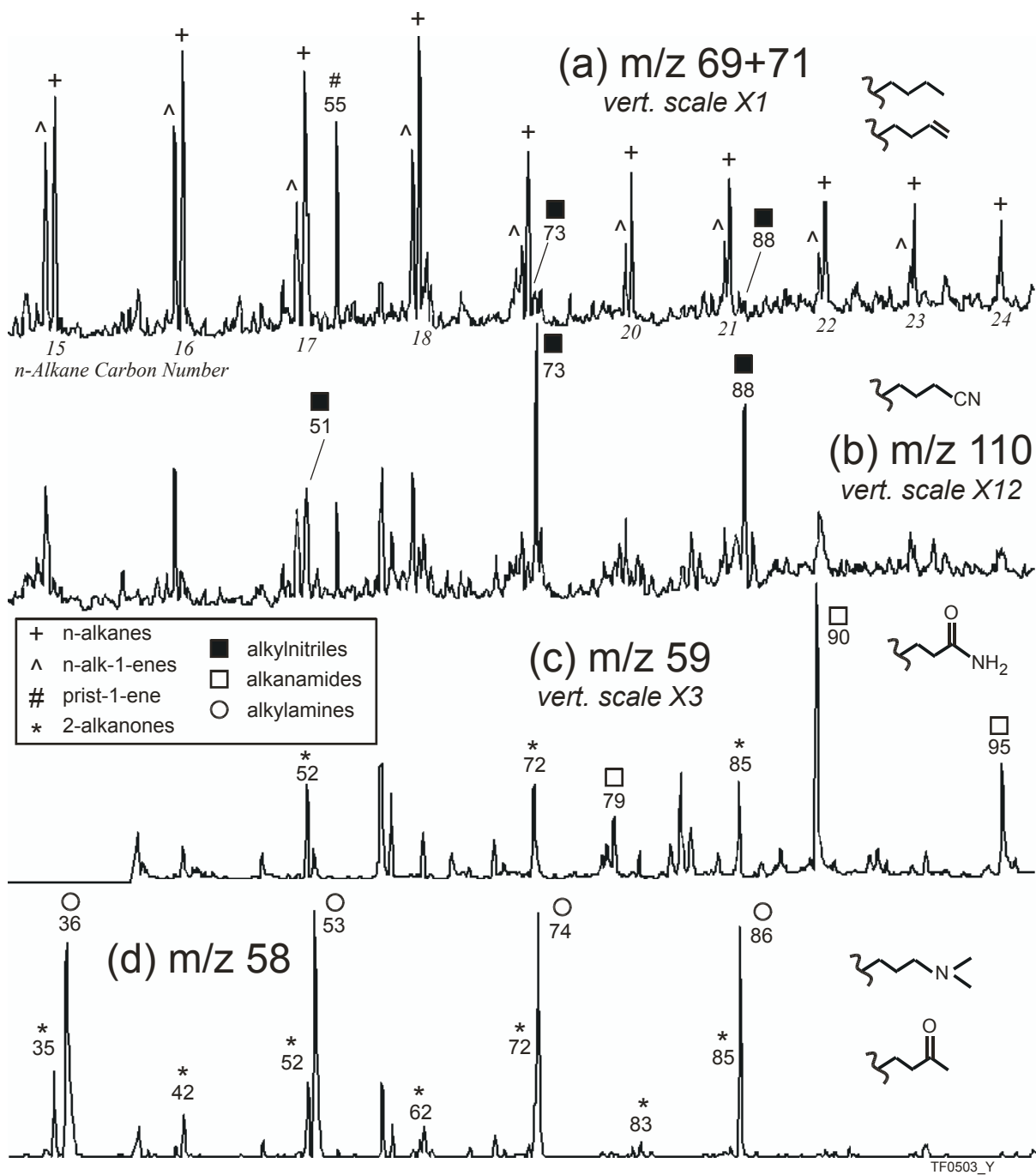
[Figure 6]

Figure 6. Mass chromatograms recorded in selected ion monitoring mode showing the distribution of significant long-chain alkyl compounds in the pyrolyzate of sample 503. See Table 2 for peak number assignments. a) C₁₅-C₂₄ *n*-alkanes and *n*-alk-1-enes (m/z 69 + 71). b) C₁₄, C₁₆ and C₁₈ *n*-alkylnitriles (m/z 110). c) C₁₄, C₁₆ and C₁₈ *n*-alkylamides and C₁₅, C₁₇ and C₁₉ *n*-alk-2-ones (m/z 59). d) C₁₂, C₁₄, C₁₆ and C₁₈ N,N-dimethyl-*n*-alkylamines and C₁₃-C₁₉ *n*-alk-2-ones (m/z 58).

The four trialkylamines detected have been in common use in the manufacture of surfactants as well as other industrial products and are regulated as hazardous substances [29]. Trialkylamines have been used as marker compounds for sewage contamination in coastal environments, originating as impurities in cationic surfactants in household cleaning products [30-35]. The trialkylamines are more hydrophobic than the related surfactant DTDMAC (ditallowdimethylammonium chloride) and degrade less readily in the environment [32-34]. The above-cited authors report the occurrence of long chain dimethylamines in marine sediments and particulate matter with C₁₄, C₁₆ or C₁₈ alkyl chains. In the present study, it is notable that the sludge pyrolyzate also contains a fourth compound, with a C₁₂ alkyl chain. The cited authors detected compounds in the form CH₃NR₁R₂ as well, for which R₁ and R₂ are C₁₄, C₁₆ or C₁₈ alkyl chains. However these larger compounds were not observed in the sludge pyrolyzates in the present study. Nevertheless, it is evident that sediment Py-GC/MS provides a direct, rapid analytical method for detection of trialkylamine marker compounds without the need for expensive and time-consuming sample preparation procedures.

While long chain amides and nitriles are intermediates in the manufacture of trialkylamines [36], other origins are possible under flash pyrolysis conditions. The alkylnitrile and alkylamide series are likely to be microbial marker compounds in these pyrolyzates [5,16,37-41]. Oros and Simoneit [42] proposed a pyrolytic origin for alkylnitriles detected in the combustion products of various types of biomass. Cao and co-workers [24] suspected that alkylnitriles and alkylamides detected in sewage sludge pyrolyzates were formed via reactions of fatty acids with ammonia. The alkylamides are in fact major components of the pyrolyzate of freeze-dried cultured *E. coli* (C₁₆ > C₁₄ > C₁₈) and the C₁₆

Fig. 6



alkylnitrile is also present. In the experiment involving thermodesorption of sample 503 at 300 °C followed sequentially by pyrolysis of the same aliquot at 610 °C, the majority of the two lower molecular weight trialkylamines (**36**, **53**) were released at the lower temperature, along with a lesser fraction of the two higher molecular weight homologues. The remaining amounts of these four compounds were released at 610 °C. In contrast, the alkylnitriles and alkylamides were only produced at the higher temperature. The trialkylamines are evidently present as free or loosely bound compounds in the sediments, whereas the alkylnitriles and alkylamides are true biomass pyrolysis products.

3.2.3.2 Steroids

One of the most striking features of the sample 503 pyrogram is the cluster of prominent peaks (**98-117**) in the *n*-C₂₈ - *n*-C₃₁ elution range (Figs. 5a, 7a). Of the compounds these peaks represent, the sterenes are the most abundant, with C₂₇ > C₂₉ > C₂₈ (Fig. 7a; b) and at least 4 isomers for each carbon number, in relatively the same proportions, as evidenced on the mass chromatograms of the respective molecular ions (Fig. 7e). The strong *m/z* 316 fragment (M⁺ -54) for two C₂₇ sterenes (**99**, **100**) leads to their identification as cholest-2-enes [43,44], likely 5 α (H) and 5 β (H). The M⁺ -54 fragments at *m/z* 330 and 344 are analogous for C₂₈ and C₂₉ Δ^2 sterenes (Fig. 7f). Kruge and Permanyer [5] recognized sterenes in the pyrolyzate of Barcelona harbor sediments and attributed them to sewage pollution in the inner harbor. The *m/z* 217 trace shows the distribution of the C₂₇-C₂₉ steranes, as well as minor peaks corresponding to the sterenes (Fig. 7c). For each carbon number the 5 α (H), 14 α (H), 17 α (H) 20R stereoisomer (**102**, **108**, **112**) is strongly predominant. This indicates thermal immaturity in the petroleum geochemical sense [45] and implies that direct petroleum contamination, while present as noted above, is not a major factor in this waste stream. If the steranes were derived from petroleum, then most likely they would exhibit a thermally mature stereoisomer distribution. C₂₇ and C₂₉ steradienes (**103**, **116**) are present at relatively lower abundances (Fig. 7a; g); no C₂₈ steradiene was detected. A C₂₇ stanone (**117**), tentatively identified as coprostanone (5 β -cholestan-3-one), and, most tellingly, the mammalian fecal C₂₇ steroid coprostanol (5 β -cholestan-3 β -ol) (**115**) are present in relatively high abundances (Fig. 7a; d). Cholesterol (cholest-5-ene-3 β -ol) was not detected.

[Figure 7]

Figure 7. Mass chromatograms showing the C₂₇ – C₂₉ steroids detected in the pyrolyzate of sample 503, typical for sewage sludge. Full scan; Thermo Finnegan instrument. See Table 2 for peak number assignments. MS ions used and vertical scaling factors (relative to the total ion current trace) are given for each trace. a) total ion current. b) *m/z* 215 showing the C₂₇ – C₂₉ steradienes. c) *m/z* 217 showing C₂₇ – C₂₉ steranes. d) *m/z* 388 and 386, molecular ions for coprostanol and a C₂₇ stanone, respectively. e) *m/z* 370, 384 and 398, the molecular ions for the C₂₇, C₂₈ and C₂₉ sterenes, respectively. f) *m/z* 316, 330 and 344, characteristic M⁺ -54 fragment ions for the C₂₇, C₂₈ and C₂₉ ster-2-enes, respectively. g) *m/z* 368 and 396, the molecular ions for C₂₇ and C₂₉ steradienes, respectively.

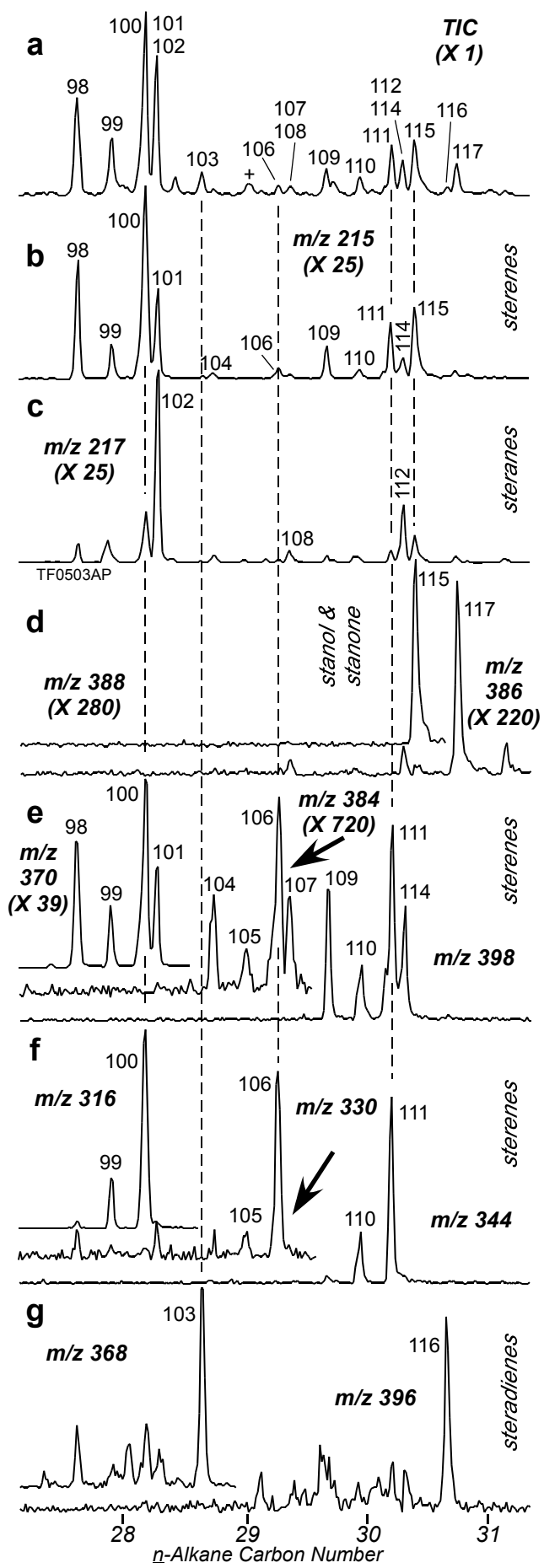


Fig. 7

Coprostanol is commonly used as a marker compound for sewage pollution as it is formed in the mammalian gut by the microbial reduction of cholesterol [34,35,46-49]. In an assessment of sewage pollution in the western Mediterranean Sea, Maldonado and coworkers [34] found that the highest concentrations of coprostanol were in suspended matter collected near the mouth of the Besòs River, near the present study area. In a survey of ocean bottom sediment pollution, Maldonado and others [35] detected very high coprostanol concentrations near a similar marine sewage plant outfall in California. The authors of both studies also noted elevated trialkylamine concentrations in these samples. It would be expected therefore that coprostanol and the related steroid coprostanone would be abundant in the pyrolyzates of sewage sludge itself, likely as direct thermodesorption products. While these compounds are indeed present, the predominant steroids in the pyrolyzate are hydrocarbons, particularly the sterenes (Fig. 7). Sterenes have been known for some time to occur in marine sediments and immature organic-rich rocks [43,50], but are not reported in the above cited studies examining coprostanol as a sewage pollution marker. Confined and hydrous pyrolysis of cholesterol under a variety of conditions produces abundant Δ^4 and Δ^5 cholestenes, along with cholestadienes and cholestane [51,52]. These authors did not report Δ^2 sterenes, however their starting material (cholest-5-ene-3 β -ol) is a Δ^5 steroid. It is most likely that the sterenes and steradienes present in the sewage sludge pyrolyzate are thermal alteration products of steroid alcohols, with the strong C₂₇ predominance (Fig. 7) and the presence of coprostanol itself suggesting coprostanol as the primary precursor. We therefore propose the use of this sterene distribution pattern (C₂₇ > C₂₉ > C₂₈; Fig. 7) as a Py-GC/MS signature for sewage pollution in sediments.

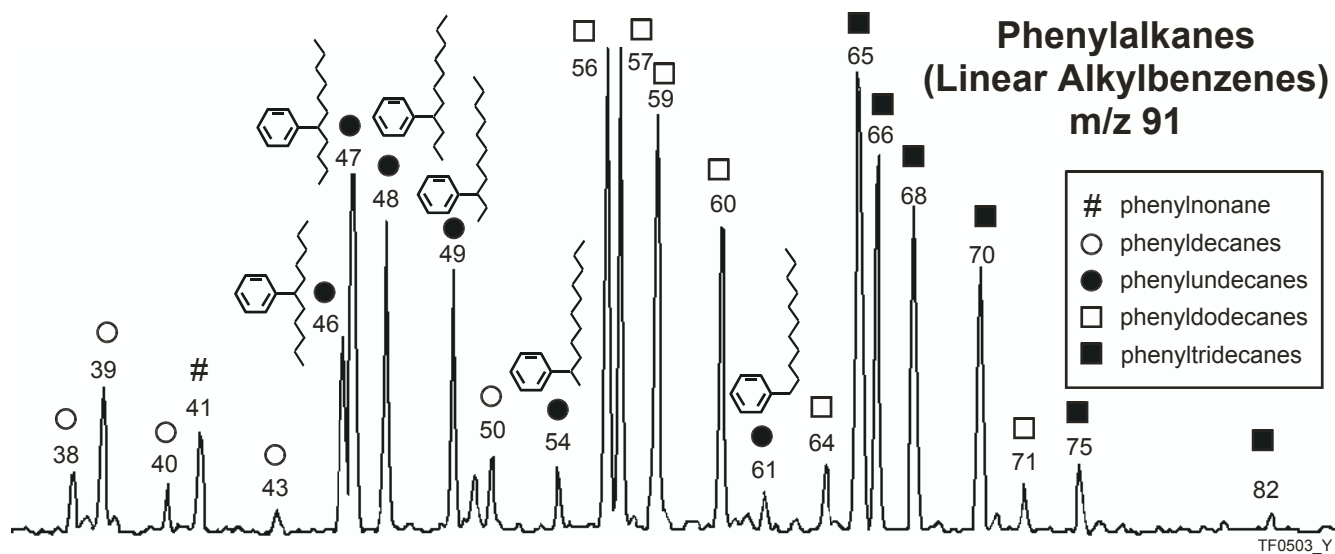
3.2.3.3. Linear alkylbenzenes

The third compound class of interest in the sewage sludge pyrolyzates is the linear alkylbenzenes (LABs), well known as persistent marker compounds for synthetic linear alkylbenzene sulfonate surfactant discharges into the aquatic environment [32,33,53-55]. We have previously reported the occurrence of LABs in the pyrolyzate of a contaminated sediment sample from inner Barcelona harbor [5]. In that case, there were only the three mid-chain isomers (6-, 5-, and 4-phenylalkanes) detected for each carbon number (side chain carbon number $n = 10$ to 13 in C₆H₅ - C_nH_{2n+1}). In contrast, the pyrolyzates of the sewage sludge show the full series of 6 isomers, with the phenyl substitution occurring at positions 6 through 1 on the alkyl chain (Fig. 8). The presence of the end-chain isomers may indicate better LAB preservation and/or more recent deposition in the sludge deposit [55], although this interpretation should be made with caution [56]. Regardless, the LABs are readily detected by Py-GC/MS. Thermodesorption at 300 °C produced about one third as much of the LAB yield as did the sequential pyrolysis at 610 °C of the same sample aliquot, but the isomer and homologue distributions were the same under both temperature conditions. We conclude that the LABs are present as free or loosely bound compounds in the sludge.

[Figure 8]

Figure 8. Mass chromatogram recorded in selected ion monitoring mode showing the distribution of C₁₅-C₁₉ linear alkylbenzenes (LABs) in the pyrolyzate of sample 503. See Table 2 for peak number assignments. As examples, the structures are shown for the six phenylundecane isomers.

Fig. 8



3.2.4. Principal components analysis

Rock Eval, elemental, and Py-GC/MS analyses yielded a total of 135 variables for each of 44 samples (Table 1 and quantified compounds in Table 2). Principal components analysis (PCA) provides a convenient means to discern trends in this large dataset, as was done in our previous study of Barcelona harbor sediments [5]. In the initial PCA experiment, the first and second principal components accounted for 51 and 12 % of the variance in the data set, respectively. As in our Barcelona harbor study, examination of the corresponding eigenvectors revealed that related variables (e.g., the individual linear alkylbenzenes from the Py-GC/MS results) had very similar values. Combining some variables (related organic compounds) and eliminating others (elements showing little variation) permitted simplification, reducing the number of variables to 60 (Table 3). The subsequent PCA experiment using these 60 variables produced first and second principal components also accounting for 51 and 12 % of the variance. The relative positions of the samples within the first and second principal components are essentially the same for both experiments, validating the variable reduction exercise. Only the first principal component from the latter experiment will be discussed further, since it explains most of the variance.

[Table 3]

Table 3. Variables used in principle components analysis. The values are the contribution of each to the eigenvector of the first principal component. Using the group codes, refer to Table 2 to see the compounds comprising each group.

Many of the 60 variables in the second PCA experiment make large, positive contributions to the eigenvector of the first principal component (Table 3), for example, total organic carbon, calcium, phosphorus, silver, Rock Eval S₂ and hydrogen index, indoles, and the alkyl nitrogen compounds. The Rock Eval oxygen index and elements such as aluminum and iron make large negative contributions. Elevated C_{org}, Ca, and S₂ values are clearly associated with the sewage sludge deposit samples (Fig. 3, Table 1). The PCA results indicate that the other variables with large positive contributions to the eigenvector of the first principal component are likely also significant in the sludge deposit, whereas the variables with large negative contributions tend to be associated with the uncontaminated sediments.

3.3 Biomarkers in the geospatial context

Considering the map coordinates of each core location and the sediment depths, the ten cores effectively constitute a three-dimensional (3-D) sample set. It is desirable to be able to visualize the analytical results in this geospatial context, which will ultimately benefit remediation efforts. A geographic information system provides effective tools to do so, allowing one to observe variations with depth in the cores, using standard graphical representations. For example, in core 5, from the thickest part of the sludge deposit, there are elevated C_{org} concentrations within the sludge in the upper part of the core, diminishing sharply at ca. 105 cm (Fig. 9a), corresponding to the downcore transition from dark to light-

Table 3.

Variable	Group Code	Value	Variable	Group Code	Value
Organic Carbon		0.174	Hopanes	HO	0.113
Rock Eval S2		0.172	Furfurals	FR	0.111
Silver		0.171	Barium		0.109
Linear Alkylbenzenes	LAB	0.165	Sulfur		0.103
Rock Eval TOC		0.165	Dibenzothiophene		0.101
Zinc		0.164	Pyrroles	PL	0.093
Copper		0.163	Sterenes & Steranes	ST	0.093
n-Alkanes	AL	0.160	C2- & C3-Naphthalenes	N	0.088
Rock Eval S3		0.160	2-Methylnaphthalene		0.079
Indoles	IL	0.160	Pyrenes & Isomers	PY	0.076
Phosphorus		0.159	C1- & C2-Phenols	F	0.073
Calcium		0.157	Boron		0.063
Strontium		0.156	Prist-2-ene		0.048
Sodium		0.154	Toluene		0.000
Alkylamines	AA	0.154	Chrysene & Benzo[a]anthracene	CH	-0.005
1-Methylnaphthalene		0.152	Naphthalene		-0.006
Rock Eval S1		0.150	Rock Eval Oxygen Index		-0.092
Cadmium		0.143	Arsenic		-0.092
Nickel		0.143	Pyridines	PD	-0.100
Alkyl nitriles	AN	0.142	Methylthiophenes	T	-0.102
Alkylamides	AM	0.141	Phenol		-0.117
Prist-1-ene		0.139	Titanium		-0.118
Dihydrobenzofuran		0.133	Cobalt		-0.123
Lead		0.131	Magnesium		-0.136
Guaiacol		0.129	Aluminum		-0.139
Triaromatics	PA	0.128	Potassium		-0.139
Chromium		0.124	Manganese		-0.144
Cyclopentenones	CP	0.121	Iron		-0.149
Rock Eval Hydrogen Index		0.114	Beryllium		-0.151
Styrene		0.113	Zircon		-0.160

colored sediment at the base of the sludge deposit (Fig. 2). As noted above (Table 1) and emphasized in the PCA results (Table 3), the concentrations of a number of elements and certain Rock Eval parameters behave in this way, for example P, Ag, and S₂ (Figs. 9b-d). Similarly, the relative enrichment in linear alkylbenzenes and organonitrogen compounds is clearly evident in the sludge (Figs. 9e, 9f). The enrichment in steroids is less clear-cut (Fig. 9g), indicating some heterogeneity within the sludge deposit. The first principal component accounted for most of the variance and its values toggle from positive to negative with depth in the core. (Fig. 9h).

[Figure 9]

Figure 9. Changes with depth observed in Core 5 for eight geochemical parameters. a) Organic carbon. b) Phosphorus. c) Silver. d) Rock Eval S₂. e) “Excess” linear alkylbenzenes. f) “Excess” organonitrogen compounds. g) “Excess” sterenes and steranes. . h) First principal component. “Excess” values derive from the semi-quantitative Py-GC/MS results corrected for MS response and normalized to toluene, as described in the text.

¹Sum of linear alkylbenzenes / toluene

²(indoles + alkylnitriles + alkylamides + alkylamines) / toluene

³Sum of C₂₇-C₂₉ sterenes & steranes / toluene

Table 2 lists the specific compounds employed and the MS ions used in their quantitation. Variables used in principal component analysis given in Table 3.

For a 3-D visualization of the results, we modified the above simple graphical approach. We subdivided the study area’s sediment pile into 12 stacked slices of uniform (20 cm) thickness, based on the distribution of available core subsamples (Table 1), with the sediment-water interface as the datum. The magnitude of a parameter in a given slice at each core site is proportional to the length of the “flag” (bar) attached at the corresponding slice depth to the line symbolizing that core on the map. The resulting “flag plots” correspond to the standard depth plots as shown in the example (Fig. 10).

[Figure 10]

Figure 10. Evolution of graphic representational model used in 3-D geochemical mapping. a) Standard graph of C_{org} as a function of sediment depth, as in Figure 9a. b) Bar graph (“flag plot”) presentation of the same data generalized in 20 cm vertical slices; null values indicate absence of data. See text for fuller explanation.

The flag plots for all ten cores can now be displayed for any desired geochemical parameter in a compact form, using the sample location map (Fig. 1) as the base map. The distribution of C_{org} is thus effectively displayed in Figure 11a, for which the maximum flag length corresponds to a C_{org} value of 5.9%, i.e., for the 0-20 cm slice encountered in core 5. With this visual perspective, it is clearly evident that the upper portions of cores 2 and 5, adjacent to the mud pipe in the main sludge mound, record the greatest C_{org} enrichment. The upper portions of cores 6 and 7, in the smaller northwestern mound, and cores 3 and 4, on the

Core 5

Fig. 9

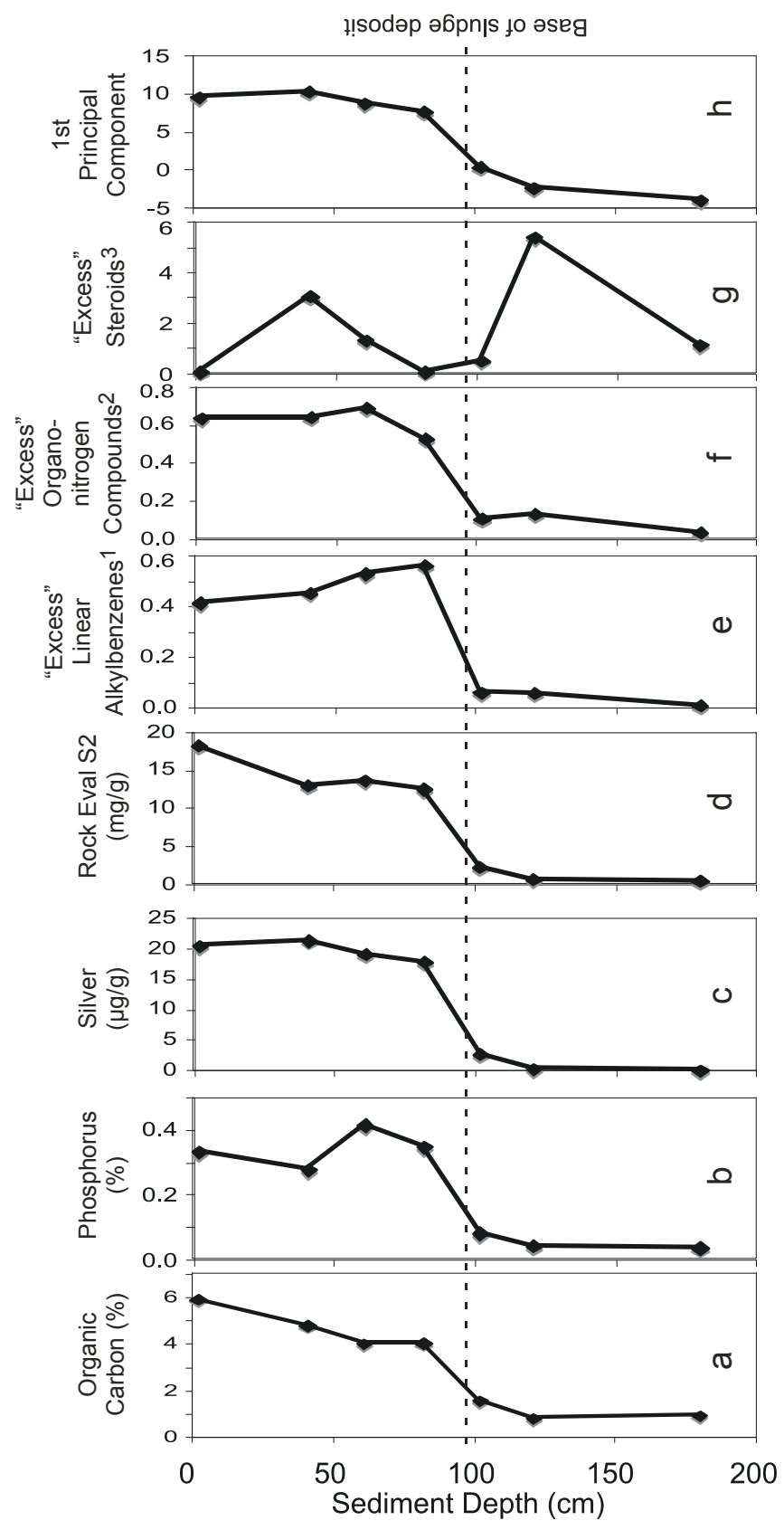
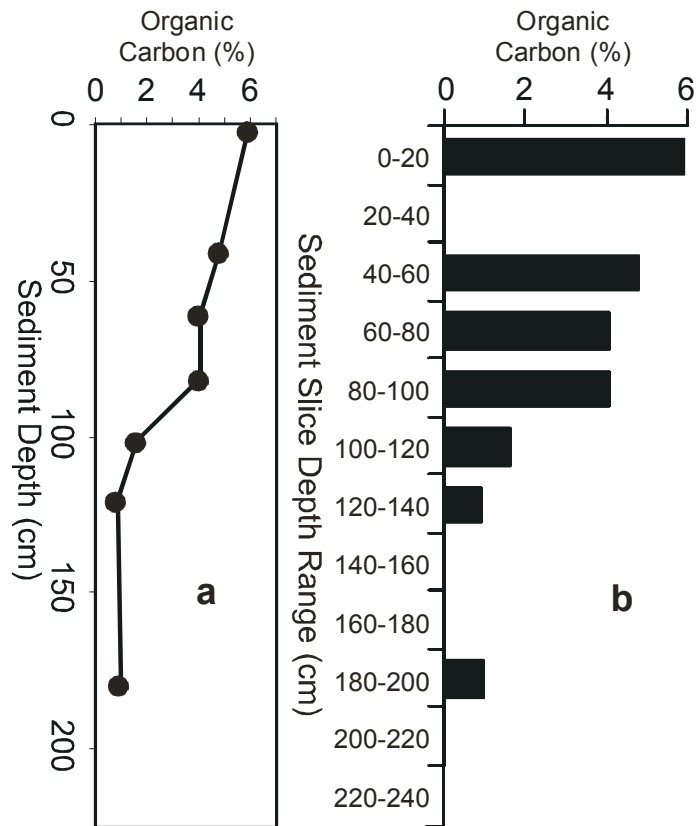


Fig. 10



southwestern margin of the main body, also record the impact, but to a lesser degree. The uppermost segment of core 9 also exhibits elevated C_{org} values, remarkable since this core was taken about 1500 m southwest of the main sludge mound. As was noted above, the southwesterly bulge of the surface sediment Ca^{2+} concentration isopleths and the double lobe feature on the sludge margin southwest of core 5 are evidently in response to the prevailing southwesterly marine current (Fig. 1). The lobes are likely adjacent to a particularly large rupture in the mud pipe. The current has evidently transported some sludge upon its initial release, since once it has been deposited, its cohesiveness renders it resistant to resedimentation. Core 8, although closer to the sludge deposit than core 9, exhibits only a slight increase in C_{org} in its uppermost layer, suggesting that pipe rupture was less of a problem in its vicinity. Distal cores 1 and 10 show little increase in C_{org} above background and are thus relatively unaffected by the sludge deposit (Fig. 11a).

[Figure 11]

Figure 11. Maps showing the values of eight geochemical parameters at each of the ten core locations, plotted as a function of sediment depth using “flag plots” as in Figure 10b. Within each figure the vertical and horizontal scales are constant; null values indicate absence of data. The base map is derived from Figure 1 and shows sludge deposit boundaries, disposal pipes and bathymetric contours. See text for explanation. a) Organic carbon. b) Phosphorus. c) Silver. d) Rock Eval S_2 . e) “Excess” linear alkylbenzenes. f) “Excess” organonitrogen compounds. g) “Excess” sterenes and steranes. h) First principal component. “Excess” is defined in the text and is as used in Figure 10. Variables used in principal component analysis given in Table 3.

Phosphorus and silver concentrations, as well as Rock Eval S_2 values, show a similar spatial arrangement: most elevated in the upper portions of cores 2 and 5, as well as moderate enrichment at the top of cores 3, 4, 6, and 9, while cores 1, 8 and 10 appear nearly unaffected by the sludge (Figs. 11b-d). Significant LAB enrichment is only evident in the upper portions of cores 2, 5 and 6, as well as in the top sediments of cores 3 and 4 (Fig. 11e). Only minor LAB enrichment is seen in the upper portion of core 7. The spatial distribution of excess organonitrogen compounds (Fig. 11f) closely resembles that of C_{org} (Fig. 11a), with the greatest enrichment along the spine of the sludge deposit. The most extreme steroid enrichment is evident within the main mound of the sludge deposit, while the effect is fainter on the margins (Fig. 11g). In Figure 11h, the spatial distribution of the first principal component values makes a remarkably sharp distinction between sludge contamination (positive values) and the relatively uncontaminated background (negative), with the largest positive values found nearest to the ruptured mud pipe. This latter map provides a particularly effective means of visualizing the extent of the pollution problem and should be especially useful in remediation planning. Since the geochemical contrast between the sludge and the basal sediments is so pronounced, the first principal component in this case accounted for an extraordinarily large fraction of the variance in the dataset. By itself, it suffices to delineate the affected sediment in 3-D.

Fig. 11a-d

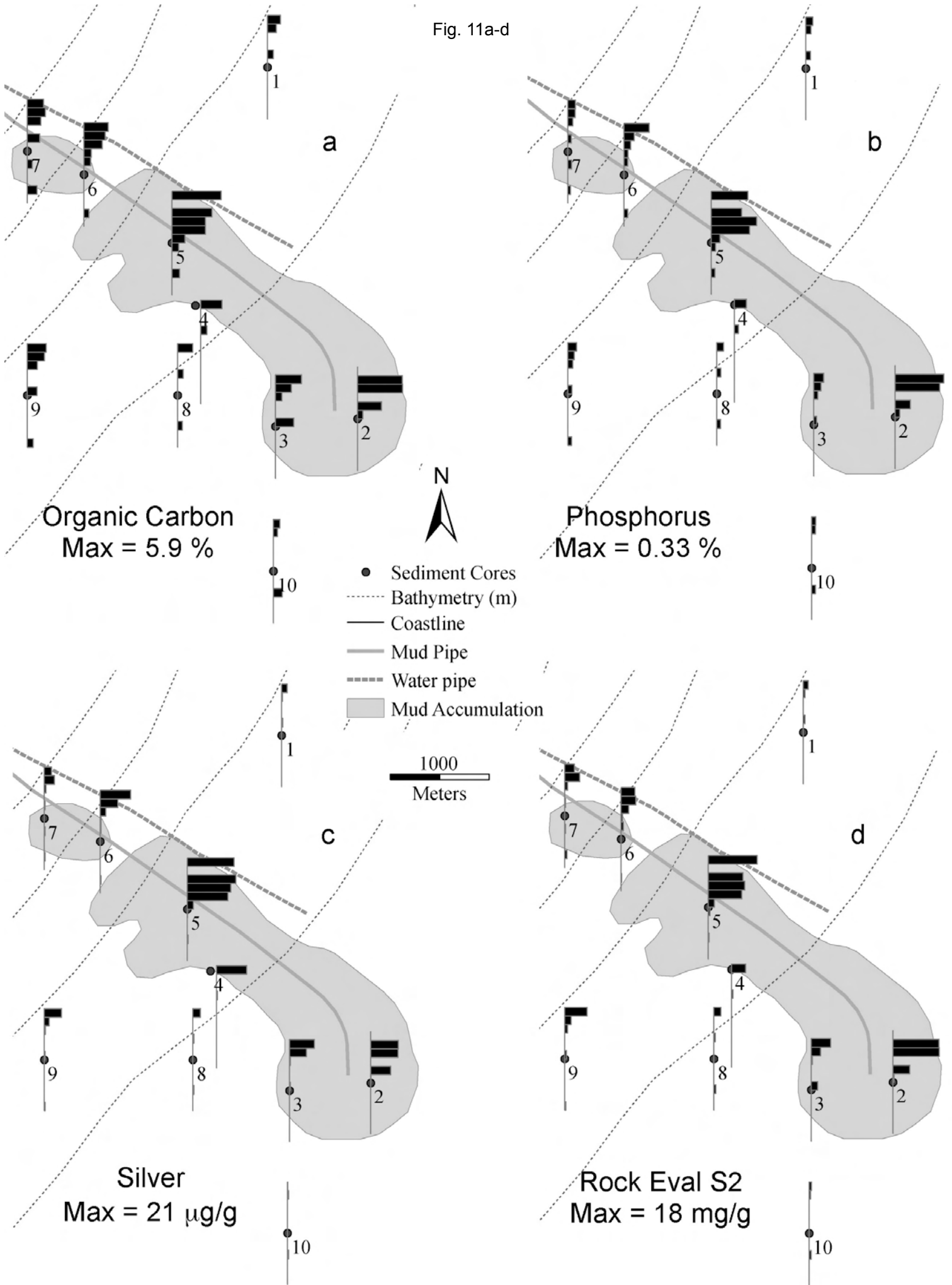
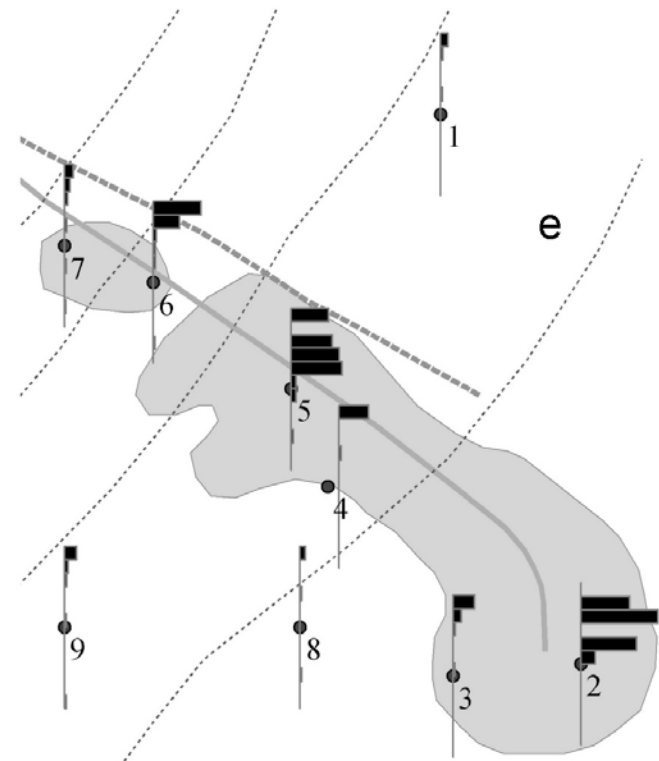
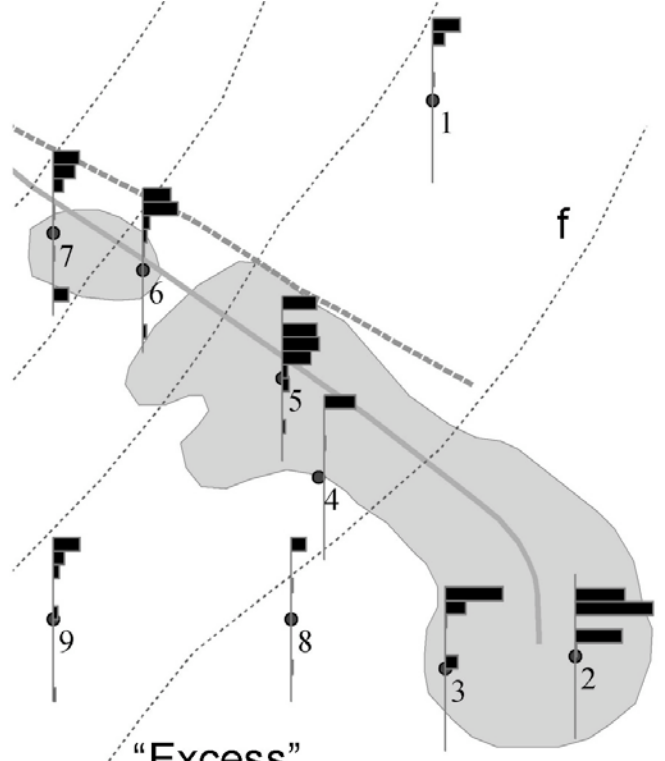


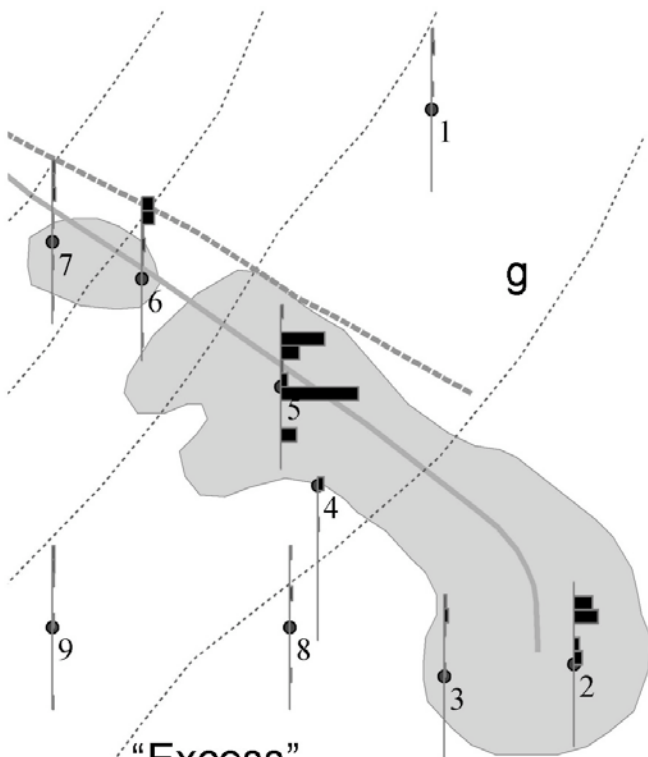
Fig. 11e-h



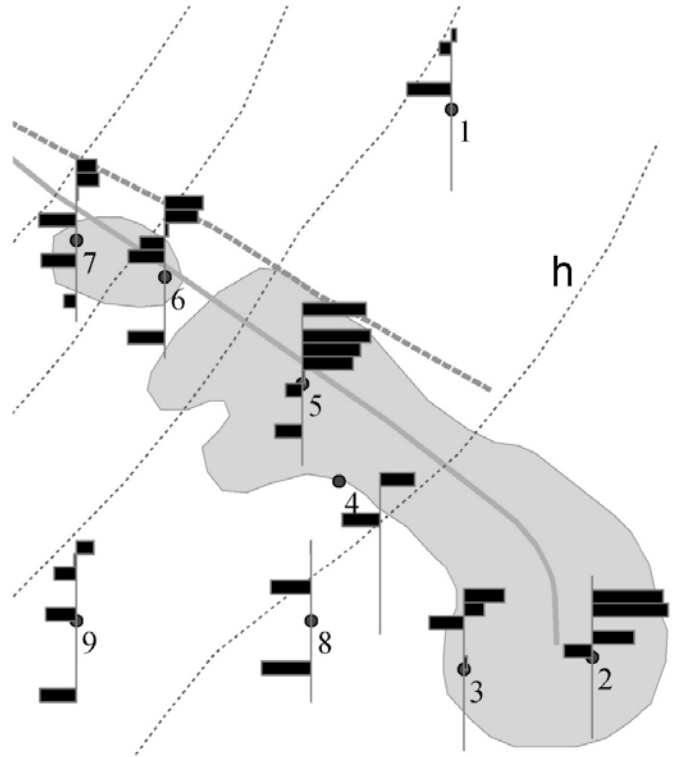
**“Excess”
Linear Alkylbenzenes
(LABs / Toluene
by Py-GC/MS)
Max = 0.84**



**“Excess”
Organonitrogen
Compounds
(ONCs / Toluene
by Py-GC/MS)
Max = 1.40**



**“Excess”
Sterenes & Steranes
(Steroids / Toluene
by Py-GC/MS)
Max = 5.37**



**1st Principal
Component
Max = +11.5**

4. Conclusions.

High resolution seismic reflection data were used to estimate the extent and thickness of the sludge deposit, based on the contrast between its signature and that of the surrounding sediments. The sludge was further mapped based on its chemical characteristics. Elemental analysis indicated enrichment in C_{org} , Ca, Na, P, and S, all derived from the organic constituents of the sewage or substances added during sewage treatment, as well as in trace elements of industrial provenance such as Ag, Cr, Cu, Pb, and Zn. Rock Eval pyrolysis, normally used as a tool in petroleum prospecting, was shown to offer a simple means to effectively delineate the sludge deposit, with the S_2 parameter and the hydrogen and oxygen indices particularly useful.

For more detailed characterization of the sludge deposit on the molecular level, sediment Py-GC/MS provided a direct, rapid analytical method for detection of an extensive suite of sewage marker compounds, without the need for expensive and time-consuming sample preparation procedures. Characteristic marker compounds included C_{16} - C_{19} linear alkylbenzenes (LABs), indole, methylindole, and diketopiperazines, as well as long-chain alkylnitriles, alkylamides, and trialkylamines. The LABs and trialkylamines are known surfactant marker compounds, while the other nitrogen compounds are most likely pyrolysis products of biomass present in the sludge. Of particular interest, the sludge pyrolyzates contained the fecal sterol coprostanol and pyrolytic steroid derivatives, of which sterenes are the most important. We propose the use of the observed sterene carbon number distribution pattern ($C_{27} > C_{29} > C_{28}$) as a Py-GC/MS signature for sewage pollution in sediments. The recognition of the pyrolysis-GC/MS and Rock Eval signatures in this deposit will facilitate the use of this method in the detection of sewage-contaminated sediments in urban waterways worldwide.

Principal components analysis aided the interpretation of the large geochemical dataset and the use of a geographic information system enabled the three-dimensional visualization of the results in their geospatial context. The distinctive pyrolysis products and the trace elements are geochemical markers which would be useful in planning and assessing the efficacy of any future remediation program.

Acknowledgements

The study was partially funded the Spanish Ministry of Education and Science (Grant CGL2006-05491/BTE). This is contribution number PSEG ISS-10-0041 from the Montclair State University PSEG Institute for Sustainability Studies. We thank the two anonymous reviewers for their constructive and helpful comments.

References

- [1] J. Piskorz, D.S. Scott, I.B. Westerberg, Flash pyrolysis of sewage sludge, *Ind. Eng. Chem. Proc. D. D.* **25** (1986) 265-270.
- [2] J.A. Caballero, R. Front, A. Marcilla, J.A. Conesa, Characterization of sewage sludges by primary and secondary pyrolysis, *J. Anal. Appl. Pyrol.* **40-41** (1997) 433-450.

- [3] A. Domínguez, J.A. Menéndez, M. Inguanzo, J.J. Pís, Production of bio-fuels by high temperature pyrolysis of sewage sludge using conventional and microwave heating, *Bioresource Technol.* **97** (2006) 1185-1193.
- [4] M. Ischia, C. Perazzolli, R. Dal Maschio, R. Campostrini, Pyrolysis studies of sewage sludge by TG-MS and TG-GC-MS coupled analyses, *J. Therm. Anal. Calorim.* **87** (2007) 567-574.
- [5] M.A. Kruge, A. Permanyer, Application of pyrolysis-GC/MS for rapid assessment of organic contamination in sediments from Barcelona harbor, *Org. Geochem.* **35** (2007) 1395-1408.
- [6] J. Serra, J. Salat, A. Cruzado, Essai d'utilisation des sédiments superficiels comme indicateurs de la distribution de la pollution au large de Barcelona, *Journées des Études des Pollutions CIESM 5* (1980) 949-952.
- [7] J. Espitalié, J.L. Laporte, M. Madec, F. Marquis, P. Leplat, J. Paulet, A. Boutefeu, Méthode rapide de caractérisation des roches mères de leur potentiel pétrolier et de leur degré d'évolution, *Rev. Inst. Fr. Pétrol.* **32** (1977) 23-42.
- [8] J. Espitalié, G. Deroo, F. Marquis. La pyrolyse Rock-Eval et ses applications. Part I, *Rev. Inst. Fr. Pétrol.* **40** (1985) 563-578.
- [9] J. Espitalié, G. Deroo, F. Marquis. La pyrolyse Rock-Eval et ses applications. Part II, *Rev. Inst. Fr. Pétrol.* **40** (1985) 755-784.
- [10] J. Espitalié, G. Deroo, F. Marquis. La pyrolyse Rock-Eval et ses applications. Part III, *Rev. Inst. Fr. Pétrol.* **41** (1986) 73-89.
- [11] K.E. Peters, Guidelines for evaluating petroleum source rock using programmed pyrolysis, *AAPG Bull* **70** (1986) 318-329.
- [12] M.A. Kruge, P.K. Mukhophadyay, C.F.M. Lewis, A molecular evaluation of contaminants and natural organic matter in surface sediments from western Lake Ontario, *Org. Geochem.* **29** (2007) 1797-1812.
- [13] P.A. Meyers, H. Doose, Sources, preservation, and thermal maturity of organic matter in Pliocene-Pleistocene organic carbon-rich sediments of the western Mediterranean Sea, in: R. Zahn, M.C. Comas, A. Klaus (Eds.), *Proceedings of the Ocean Drilling Program, Scientific Results*, **161** (1999) 383-390.
- [14] C. Marchand, E. Lallier-Vergès, J.R. Disnar, D. Kéravis, Organic carbon sources and transformations in mangrove sediments: A Rock Eval pyrolysis approach, *Org. Geochem.* **39** (2008) 408-421.
- [15] I.C. Smith, B.L. Carson, *Trace metals in the environment, Volume 2, Silver*, Ann Arbor Science Publishers, Ann Arbor, 1977.
- [16] M.-A. Sicre, S. Peulvé, A. Saliot, J.W. de Leeuw, M. Baas, Molecular characterization of the organic fraction of suspended matter in the surface waters and bottom nepheloid layer of the Rhone delta using analytical pyrolysis, *Geochim. Cosmochim. Ac.* **21** (1994) 11-26.
- [17] S. Peulvé, J.W. de Leeuw, M.-A. Sicre, M. Baas, A. Saliot, Characterization of macromolecular organic matter in sediment traps from the northwestern Mediterranean Sea, *Geochim. Cosmochim. Ac.* **60** (1996) 1239-1259.

- [18] A. Garcette-Lepecq, S. Derenne, C. Largeau, I. Bouloubassi, A. Saliot, Origin and formation pathways of kerogen-like organic matter in recent sediments off the Danube delta (northwestern Black Sea), *Org. Geochem.* **31** (2000) 1663-1683
- [19] X. Zang, P.G. Hatcher, A Py-GC-MS and NMR spectroscopy study of organic nitrogen in Mangrove Lake sediments, *Org. Geochem.* **33** (2002) 201-211.
- [20] V. Parnaudeau, M.-F. Dignac, The organic matter compositions of various wastewater sludges and their neutral detergent fractions as revealed by pyrolysis-GC/MS, *J. Anal. Appl. Pyrol.* **78** (2007) 140-152.
- [21] N. Gallois, J. Templier, S. Derenne (2007) Pyrolysis-gas chromatography-mass spectrometry of the 20 protein amino acids in the presence of TMAH. *J. Anal. Appl. Pyrolysis* 80: 216-230.
- [22] N.D. Danielson, L.B. Rogers, Determination of tryptophan in proteins by pyrolysis gas chromatography, *Anal. Chem.* **50** (1978) 1680-1683.
- [23] W.H. Marmer, P. Magidman, H.M. Farrell, Pyrolysis gas chromatography of wool. Part II: Detection and quantitation of tryptophan in wool and simple proteins, *Text. Res. J.* **59** (1989) 616-622.
- [24] J.-P. Cao, X.-Y. Zhao, K. Morishta, X.-Y. Wei, T. Takarada, Fractionation and identification of organic nitrogen species from bio-oil produced by fast pyrolysis of sewage sludge, *Bioresource Technol.* **101** (2010) 7648-7652.
- [25] B.A. Stankiewicz, J.C. Hutchins, R. Thomson, D.E.G. Briggs, R.P. Evershed, Assessment of bog-body tissue preservation by pyrolysis-gas chromatography/mass spectrometry, *Rapid Commun. Mass Sp.* **11** (1997) 1884-1890.
- [26] B.A. Stankiewicz, M. Mastalerz, C.H.J. Hof, A. Bierstedt, M.B. Flannery, D.E.G. Briggs, R.P. Evershed, Biodegradation of the chitin-protein complex in crustacean cuticle, *Org. Geochem.* **28** (1998) 67-76.
- [27] A. Camean, I. Moreno, T. Verdejo, F.J. Gonzalez-Vila, J.A. Gonzalez-Perez (2005). Pyrolytic behaviour of microcystins and microcystin-spiked algal blooms. *J. Anal. Appl. Pyrolysis* 74: 19-25.
- [28] D.L. Vaughn, M.A. Kruge, Use of Py-GC/MS analysis techniques in animal waste management: A preliminary survey of dairy manures, in: P. Landais et al. (Eds.), 20th International Meeting on Organic Geochemistry, Nancy, France, Abstracts, 2001, Vol. 2, pp. 309-310.
- [29] Procter and Gamble Chemicals, Materials Safety Data Sheet: Mixture of C₁₂-C₁₄ dimethylamine, fatty tertiary amine, AT-1270AE. MSDS Number AMINE234-1. Cincinatti, Ohio, USA, 2004.
- [30] M. Valls, J.M. Bayona, J. Albaigés, Use of trialkylamines as an indicator of urban sewage in sludges, coastal waters and sediment, *Nature* **337** (1989) 722-724.
- [31] P. Fernández, M. Valls, J.M. Bayona, J. Albaigés, Occurrence of cationic surfactants and related products in urban coastal environments, *Environ. Sci. Technol.* **25** (1991) 547-550.
- [32] N. Chalaux, J.M. Bayona, M.I. Venkatesan, J. Albaigés, Distribution of surfactant markers in sediments from Santa Monica basin, southern California, *Mar. Pollut. Bull.* **24** (1992) 403-407.

- [33] N. Chalaux, H. Takada, J.M. Bayona, Molecular markers in Tokyo Bay sediments: Sources and distribution, *Mar. Environ. Res.* **40** (1995) 77-92.
- [34] C. Maldonado, J. Dachs, J.M. Bayona, Trialkylamines and coprostanol as tracers of urban pollution in waters from enclosed seas: The Mediterranean and Black Sea, *Environ. Sci. Technol.* **33** (1999) 3290-3296.
- [35] C. Maldonado, M.I. Venkatesan, C.R. Phillips, J.M. Bayona, Distribution and trialkylamines and coprostanol in San Pedro Shelf sediments adjacent to a sewage outfall, *Mar. Pollut. Bull.* **40** (2000) 680-687.
- [36] R.G. Laughlin, Fabric softening, in: D. Rubingh, P.M. Holland (Eds.), *Cationic Surfactants: Physical Chemistry*, CRC Press, New York, 1991, pp. 449-468.
- [37] H. Goossens, J.W. de Leeuw, I.C. Rijpstra, G.J. Meyburg, P.A. Schenck, Lipids and their mode of occurrence in bacteria and sediments – I. A methodological study of the lipid composition of *Acinetobacter calcoaceticus* LMD 79-41, *Org. Geochem.* **14** (1989) 15-25.
- [38] M.E. Barrio, J.L. Liberia, L. Comellas, F. Broto-Puig, Pyrolysis-gas chromatography applied to the study of organic matter evolution in sewage sludge-amended soils using nitrogen-phosphorus, flame ionization and mass spectrometric detection, *J. Chromatogr. A* **719** (1996) 131-139.
- [39] P. Faure, F. Vilmin, R. Michels, E. Jardé, L. Mansuy, M. Elie, P. Landais, Application of thermodesorption and pyrolysis-GC–AED to the analysis of river sediments and sewage sludges for environmental purpose, *J. Anal. Appl. Pyrol.* **62** (2002) 297-318.
- [40] A. Garcette-Lepecq, C. Largeau, I. Bouloubassi, S. Derenne, A. Saliot, A. Lorre, V. Point, Lipids and their modes of occurrence in two surface sediments from the Danube delta and northwestern Black Sea: implications for sources and early diagenetic alteration: I. Carboxylic acids, *Org. Geochem.* **35** (2004) 959-980.
- [41] M.A. Kruge, A. Permanyer, J. Serra, Geochemical investigation of an offshore sewage sludge deposit, Barcelona, Catalonia, Spain, in: F.J. González-Vila, J.A. González-Pérez, G. Almendros (Eds.), *Organic Geochemistry: Challenges for the 21st Century, Book of Abstracts*, 22nd International Meeting on Organic Geochemistry, Seville, Spain, 2005, pp. 701-702.
- [42] D.R. Oros, B.R.T. Simoneit, Identification and emission factors of molecular tracers in organic aerosols from biomass burning. Part 2. Deciduous trees, *Appl. Geochem.* **16** (2001) 1545-1565.
- [43] R.B. Gagosian, J.W. Farrington, Sterenes in surface sediments from the southwest African shelf and slope, *Geochim. Cosmochim. Ac.* **42** (1978) 1091-1101.
- [44] R.P. Philp, *Fossil Fuel Biomarkers: Applications and Spectra*, Elsevier, Amsterdam, 1985.
- [45] K.E. Peters, C.C. Walters, J.M. Moldowan, *The Biomarker Guide. Volume 2, Biomarkers and Isotopes in Petroleum Systems and Earth History*, second ed., Cambridge University Press, Cambridge, 2005.
- [46] R.W. Walker, C.K. Wun, W. Litsky, B.J. Dutka, Coprostanol as an indicator of fecal pollution, *Crit. Rev. Env. Sci. Tec.* **12** (1982) 91-112.

- [47] J.O. Grimalt, P. Fernández, J.M. Bayona, J. Albaigés, Assessment of fecal sterols and ketones as indicators of urban sewage inputs to coastal waters, *Environ. Sci. Technol.* **24** (1990) 357-363.
- [48] S.M. Mudge, M.J. Bebianno, Sewage contamination following an accidental spillage in the Ria Formosa, Portugal, *Mar. Pollut. Bull.* **34** (1997) 163-170.
- [49] C. Pratt, J. Warnken, R. Leeming, J.M. Arthur, D.I. Grice, Detection of intermittent sewage pollution in a subtropical, oligotrophic, semi-enclosed embayment system using sterol signatures in sediments, *Environ. Sci. Technol.* **41** (2007) 792-802.
- [50] W. Giger, C. Schaffner, Unsaturated steroid hydrocarbons as indicators of diagenesis in immature Monterey Shale, *Naturwissenschaften* **68** (1981) 37-39.
- [51] M.M. Rhead, G. Eglinton, G.H. Draffan, Hydrocarbons produced by the thermal alteration of cholesterol under conditions simulating the maturation of sediments, *Chem. Geol.* **8** (1971) 277-297.
- [52] A.I. Rushdi, G. Ritter, J.O. Grimalt, B.R.T. Simoneit, Hydrous pyrolysis of cholesterol under various conditions, *Org. Geochem.* **34** (2003) 799-812.
- [53] R.P. Eganhouse, D.L. Blumfield, I.R. Kaplan, Long-chain alkylbenzenes as molecular tracers of domestic wastes in the marine environment, *Environ. Sci. Technol.* **17** (1983) 523-530.
- [54] H. Takada, R. Ishiwatari, Linear alkylbenzenes in urban riverine environments in Tokyo: Distribution, source and behavior, *Environ. Sci. Technol.* **21** (1987) 875-883.
- [55] H. Takada, R. Ishiwatari, Biodegradation experiments of linear alkylbenzenes (LABs): Isomeric composition of C₁₂ LABs as an indicator of the degree of LAB degradation in the aquatic environment, *Environ. Sci. Technol.* **24** (1990) 86-91.
- [56] R.P. Eganhouse, J. Pontolillo, Susceptibility of synthetic long-chain alkylbenzenes to degradation in reducing marine sediments, *Environ. Sci. Technol.* **42** (2008) 6361-6368.